Geophysical Journal International

Geophys. J. Int. (2013) doi: 10.1093/gji/ggt292

Geophysical Journal International Advance Access published August 28, 2013

Mesozoic(?) lithosphere-scale buckling of the East European Craton in southern Ukraine: DOBRE-4 deep seismic profile

V. Starostenko,[1] T. Janik,[2] D. Lysynchuk,[1] P. Środa,[2] W. Czuba,[2] K. Kolomiyets,[1] P. Aleksandrowski,[3,4] O. Gintov,[1] V. Omelchenko,[1] K. Komminaho,[5] A. Guterch,[2] T. Tiira,[5] D. Gryn,[1] O. Legostaeva,[1] H. Thybo[6] and A. Tolkunov[7]

[1]*Institute of Geophysics, National Academy of Sciences of Ukraine, Palladin Av.* 32, 03680 *Kiev, Ukraine. E-mail: dlysyn@igph.kiev.ua*
[2]*Institute of Geophysics, Polish Academy of Sciences, Ks. Janusza* 64, 01–452 *Warsaw, Poland*
[3]*Polish Geological Institute-National Research Institute, Lower Silesia Branch, Jaworowa* 19, 53–122 *Wrocław, Poland*
[4]*Faculty of Earth Sciences, University of Wrocław, Cybulskiego* 32, 50–205 *Wrocław, Poland*
[5]*Institute of Seismology, Gustaf Hällströminkatu* 2B, *P.O. Box* 68, FIN-00014, *University of Helsinki, Finland*
[6]*Geology Section, IGN, University of Copenhagen, Øster Volgade* 10, DK-1350 *Copenhagen, Denmark*
[7]*State Geophysical Enterprise "Ukrgeofizika", Sofii Perovskoy* 10, 03057, *Kiev, Ukraine*

Accepted 2013 July 18. Received 2013 July 18; in original form 2012 December 26

SUMMARY

In order to study the lithospheric structure in southern Ukraine, a seismic wide-angle reflection/refraction project DOBRE-4 was conducted. The 500-km-long profile starts in the SW from the Alpine/Variscan North Dobrudja Fold-Thrust Belt, being part of the Trans-European Suture Zone. It runs to the NE, mostly along the NW Black Sea coastal plain, towards the centre of the Precambrian Ukrainian Shield. The field acquisition in October 2009 included 13 chemical shot points with charge sizes 600–1000 kg every 35–50 km and 230 recording stations, every ∼2.5 km. The high data quality allows modelling of the *P*- and *S*-wave velocity structure along the profile. Two methods were used for the modelling of the seismic data. At first, ray tracing trial-and-error modelling was developed using arrivals of major refracted and reflected *P*- and *S*-wave phases. Next, the amplitudes of the recorded phases were analysed using finite-difference full waveform method. The resulting velocity model shows fairly homogeneous structure of the middle to lower crust both vertically and laterally. The situation is different in the upper crust, with V_p velocities decreasing upwards from *ca*. 6.35 at 15–20 km to 5.9–5.8 km s^{-1} at the top of the crystalline basement and to *ca*. 5.15–3.80 km s^{-1} in Neoproterozoic and Palaeozoic and to 2.70–2.30 km s^{-1} in Mesozoic strata. Below the upper crust the V_p smoothly increases downward, from *ca*. 6.50 to 6.7–6.8 km s^{-1} near the crustal base, making it difficult to differentiate between the middle and lower crust. No V_p velocities exceeding 6.80 km s^{-1} have been recorded even in the lowermost part of the crust, unlike in similar profiles on the East European Craton. There is no clear change in the velocity field when moving laterally from the Precambrian platform into the younger tectonic units to the SW. Therefore, on purely seismic grounds it is not possible to distinguish major tectonic units known from the surface. The Moho is, however, clearly delineated by a velocity contrast of *ca*. 1.3–1.7 km s^{-1}. A specific feature of the velocity model are waveform successive changes in Moho depth, corresponding to successive downward and upward bends, with wavelength of the order of 150 km and the amplitude attaining 8–17 km. Similar wavy aspect is shown by the upper mantle and upper crust, with shorter wavelength pattern in the latter. The origin of the undulations is explained by compressional lithospheric-scale buckling and ascribed to Late Jurassic–Early Cretaceous and/or end Cretaceous collision-related tectonic events associated with closing of the Palaeotethys and Neotethys oceans in this part of Europe. To our

knowledge, no such spectacular folds deforming the Moho, have been as yet revealed elsewhere by either deep reflection or refraction seismics. The presence of several detachment horizons in the folded crust calculated in the velocity model, is compatible with the existence of fold systems with various dominant wavelengths at different crustal levels. Such a situation is considered as typical of lithospheric-scale folding and reflecting the rheological stratification of the lithosphere.

Key words: Controlled source seismology; Wave propagation; Intra-plate processes; Folds and folding; Crustal structure; Europe.

1 INTRODUCTION

The lithospheric structure of the East-European Craton together with the adjacent Palaeozoic platform and Meso-Cenozoic Carpathian–Pannonian orogenic system in Central Europe have been successfully studied for decades with deep seismic methods (e.g. Grad *et al.* 2006b; Guterch *et al.* 2007). Our paper deals with results of wide-angle reflection/refraction (WARR) seismic experiment, DOBRE-4, conducted in southern Ukraine in 2009, that was aimed at investigating the gross structure of the crust and uppermost mantle at the southwestern corner of the East European Craton, at its transition into the Trans-European Suture Zone (TESZ). The WARR seismic method is a reliable and fairly accurate tool to achieve this goal through determining the distribution of seismic velocities in and thickness changes of the Earth's crust, through allocating seismic boundaries and recognizing crustal blocks delineated by deep faults, establishing waveguides, crust–mantle transient zones, and, thus, unveiling deep tectonic zonation of the upper lithosphere.

The location of the transect, along which the seismic experiment DOBRE-4 has been performed is shown in Fig. 1. The DOBRE-4 profile, approximately 500 km long, has its starting point at the Ukrainian–Romanian border near the small town of Reni on the river Danube and extends to the NE across the Black Sea coastal plain, passing *ca.* 30 km NW of Odessa and terminating north of Kryvyi Rih within gentle hills of the Dnieper Upland. DOBRE-4 is the fourth one in the series of international WARR profiles carried out in Ukraine since 1999, which have systematically studied the deep structure of the Earth's crust and upper mantle of the southern part of the East European Craton. The first 'DOBRE' experiment (DOBREfraction'99 Working Group 2003; Grad *et al.* 2003a) targeted the Donbas fold belt. The second one, DOBRE-2 was a prolongation of the DOBRE profile to the Azov massif and across the Azov Sea to the eastern Black Sea basin. The PANCAKE (DOBRE-3; Starostenko *et al.* 2013) was the third one, running from Eastern Hungary to Western Ukraine across the Carpathians.

The investigated area has been previously extensively studied by various geophysical methods, including several deep seismic sounding (DSS) profiles. The Geotraverse VIII (Sollogub *et al.* 1988) acquired in the 1970s, was located close and subparallel to the DOBRE-4 profile. It was carried out using the wide-angle and CDP seismic techniques. The Geotraverses IV and VI (Fig. 1) covered the part of the Ukrainian Shield that was later the subject of our experiment. A number of seismic soundings were performed in the Kryvyi Rih region to study the Moho boundary and construct a 3-D crustal model in the area of the Kryvyi Rih ultradeep borehole (Sharov 2004; Starostenko *et al.* 2007). The deep structure of the North Dobrudja Fold-Thrust Belt has been investigated along the VRANCEA2001 seismic line (Hauser *et al.* 2007).

All the previous investigations were focused mainly on recording the reflected seismic phases, which, unfortunately, provided only little information about the seismic velocity distribution in the lithosphere. The DOBRE-4 experiment, thanks to the usage of modern seismic stations, allowed us to obtain traveltime curves of reflected and refracted waves at offsets significantly larger than those that had been received in the past, and to produce a more detailed model of the velocity distribution and of the crustal structure.

The location of the DOBRE-4 profile is shown in Figs 1 and 2. The profile is approximately 500 km long. The field acquisition took place in the beginning of October 2009 and included 13 shot points (SP), every 30–50 km and 230 recording stations, every ∼2.5 km. 174 boreholes were used to place 8700 kg of TNT, in total. Detailed information about the shooting programme can be found in Table 1.

The project DOBRE-4 has resulted from international collaboration of institutions from Ukraine (Institute of Geophysics, National Academy of Sciences of Ukraine, and the State Geophysical Enterprise 'Ukrgeofizika', Kiev), Denmark (Geological Institute, University of Copenhagen), Finland (Institute of Seismology, University of Helsinki) and Poland (Institute of Geophysics, Polish Academy of Sciences).

2 GEOLOGICAL SETTING

The DOBRE-4 transect is located at the northwestern margin of the Black Sea (Figs 1 and 2). It starts in the SW on the Lower Prut High, representing a buried fragment of the Alpine/Variscan North Dobrudja Fold-Thrust Belt (to the east of shot point SP15100) and its foredeep, the Fore-Dobrudja Trough (between *ca.* SP15101 and SP15103), to the NE. Subsequently the transect crosses the South Ukrainian Homocline (between SP15103 and SP15108), composed of Late Neoproterozoic through Palaeozoic and Cretaceous–Neogene sedimentary cover of the south Ukrainian segment of the East European Platform. Still further to the NE it enters the Ukrainian Shield (between SP15109 and SP15112), where Proterozoic and Archaean crystalline rocks crop out at the surface (SP15110–SP15112). The transect ends near Kryvyi Rih on the Ukrainian Shield.

The transect thus spans the Precambrian East European Craton (the East European Platform and Ukrainian Shield) and its younger southwestern fringe, the Scythian Platform, with a major tectonic boundary, the Teisseyre-Tornquist Fault Zone (Guterch *et al.* 1986), on the contact with Palaeozoic and Alpine structures of Central and Southern Europe (Figs 1 and 2). Along the southwestern margin of the craton, the latter structures compose an extensive collage, named the Trans-European Suture Zone (TESZ; Pharaoh 1999), which continues NW-ward across Moldavia and western Ukraine into Poland,

Figure 1. Location of the DOBRE-4 profile and most important previous seismic experiments in the study area. Yellow stars represent shot points; grey dots show recording stations of DSS experiment; blue stars are shot points of experiments VRANCEA-2001, DOBRE-5 and registration instruments along the profile 26 (sea part of DOBRE-5); black lines with Roman numerals are old DSS Geotraverses; green lines are state boundaries. Inset map shows the location of study area in Europe. P-K, Putivl-Kryvyi Rih profile.

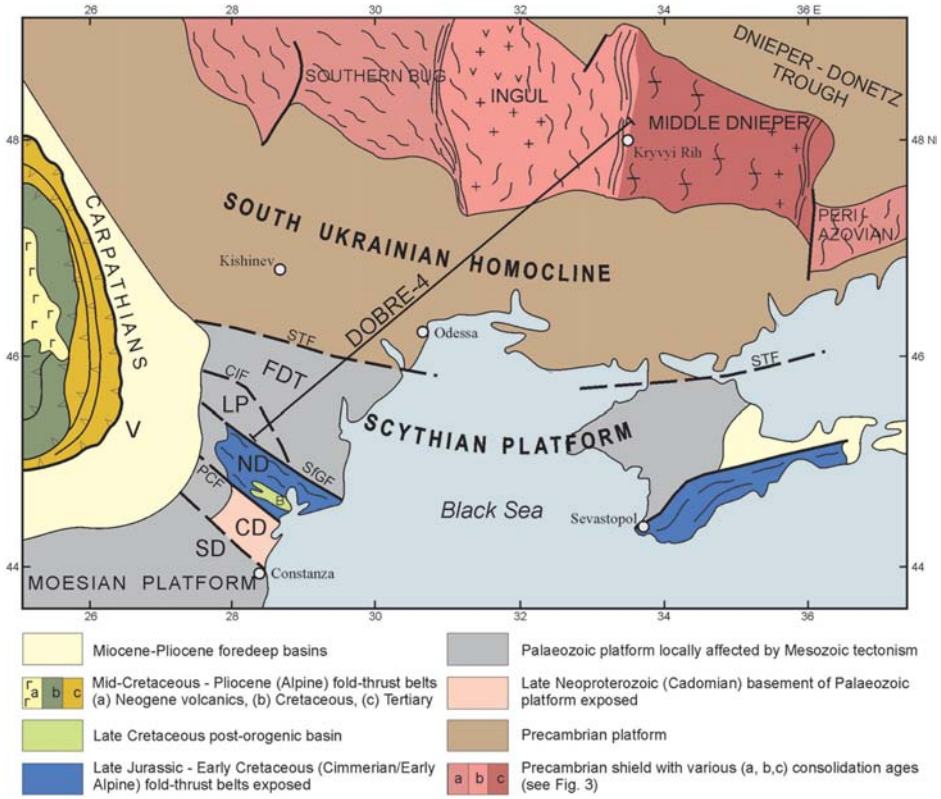

Figure 2. Tectonic setting of profile DOBRE-4. B, Babadag Basin; CD, Central Dobrudja; CIF, Cahul-Ismail Fault; FDT, Fore-Dobrudja Trough; LP, lower Prut High; PCF, Peceneaga-Camena Fault; SD, Southern Dobrudja; SfGF, Sfantu Gheorghe Fault; STF, Scytho-Turanian Fault; V, Vrancea.

Table 1. Detailed information about the shooting programme.

Shot point number	Latitude N (φ)	Longitude E (λ)	Altitude, h (m)	Time UTC (y:d:h:m:s:)	TNT charge (kg)
SP15100	45.45139	28.35333	57	2009:279:21:30:0.1	1000
SP15101	45.68194	28.7075	56	2009:279:22:30:1.2	700
SP15102	45.93222	29.12583	56	2009:280:20:30:2.72	600
SP15103	46.18667	29.54528	47	2009:281:20:30:5.1	600
SP15104	46.37194	29.9575	51	2009:279:20:0:4.7	600
SP15105	46.58694	30.34806	89	2009:279:23:0:21.75	500
SP15106	46.80694	30.73278	45	2009:279:21:8:17.35	500
SP15107	47.01722	31.14111	41	2009:281:21:30:4.38	500
SP15108	47.22444	31.55833	37	2009:282:20:1:3.15	600
SP15109	47.46889	32.06889	84	2009:281:20:0:6.98	600
SP15110	47.73222	32.53944	67	2009:280:20:0:8.56	700
SP15111	47.96889	33.02833	94	2009:279:21:59:56.09	800
SP15112	48.1775	33.44583	110	2009:279:20:30:43.13	1000

north Germany and Denmark. Approximately two thirds of the DOBRE-4 transect are located on the East European Craton.

The North Dobrudja Fold-Thrust Belt is located NE-ward of and in tectonic contact with Central Dobrudja, where Neoproterozoic (Cadomian) basement rocks of the northeastern part of the Moesian Platform are exposed (e.g. Seghedi *et al.* 2005; Oczlon *et al.* 2007). It records both Variscan and Alpine (Cimmerian) deformation, magmatism and metamorphism. Its basement comprises three metamorphic complexes, representing peri-Gondwanan terranes of Avalonian and Cadomian affinities, as well as remnants of the Palaeozoic Rheic Suture (Balintoni *et al.* 2010). The Alpine orogenic structure of North Dobrudja consists of several Cimmerian (Jurassic) thrusts sheets (Slyusar' 1984; Seghedi 2001), involving dismembered relics of a Variscan orogen and exposing a large variety of rock assemblages, including metamorphic, sedimentary and igneous complexes (Seghedi 2001, 2012; Balintoni *et al.* 2010). The metamorphic complexes comprise medium- and low-grade assemblages with sedimentary and igneous protoliths, while the sedimentary successions include late Ordovician to Devonian marine formations, Carboniferous to Early Permian clastics and volcaniclastic deposits. They are followed by Triassic, Jurassic and late Cretaceous sequences, the deposition and deformation of which witnessed the Alpine orogenic processes (e.g. Seghedi 2001, 2012; Balintoni *et al.* 2010). Igneous suites related to the Variscan and Alpine orogenies also occur there. The Triassic to Middle Jurassic sedimentation occurred in a regime of prolonged syndepositional, dextral transpression (Seghedi 2001, 2012), leading to strike-slip motions along major NW–SE trending faults, and terminated with 'Cimmerian' folding and thrusting that took place during Late Jurassic to Early Cretaceous Barremian times due to N–S directed compression (Slyusar' 1984; Hippolyte 2002). This shortening episode was repeated in the latest Cretaceous–Palaeogene under NE–SW regional tectonic compression, leading to reverse-slip reactivation of major faults and formation of large open folds in the Late Cretaceous cover (Hippolyte 2002).

To the north, across the Ismail-Cahul Fault (Slyusar' 1984), a splay of the major Sfantu Gheorghe Fault and the Teisseyre-Tornquist Fault Zone, separating the TESZ and the craton (Hippolyte 2002), the North Dobrudja Fold-Thrust Belt borders with the Fore-Dobrudja Trough (Fig. 2). The latter represents an inverted Mesozoic basin, *ca.* 120 km wide, up to 4.5 km deep, superimposed on a pre-Triassic, folded Late Neoproterozoic (Ediacaran) to Devonian strata (e.g. Seghedi 2001, 2012), resting on top of either Neoproterozoic (Cadomian) or older crystalline basement. The up to 5-km-thick sedimentary fill of the basin includes late Neoproterozoic through Permian succession with Ediacaran to Middle Silurian marine clastics, overlain by Devonian argillites and followed by carbonates and Carboniferous limestones and coal-bearing clastics. The Palaeozoic succession is terminated with Permian coarse clastics and volcanics. The Mesozoic part of the profile includes Triassic clastics and Jurassic black shales and carbonates (e.g. Gazizova 2009; Ivanova 2011). These were folded in the Late Jurassic–Early Cretaceous (*cf.* Hippolyte 2002; Gazizova 2009), though less intensely than the equivalent rock series in the adjacent North Dobrudja Fold-Thrust Belt, and became unconformably overlaid with Early Cretaceous Barremian-Albian and, then, by Late Cretaceous Cenomanian-Turonian through Palaeogene cover (Galetsky 2007; Seghedi 2012), the latter being not affected and the former little affected by folding.

The folded Palaeozoic and Late Neoproterozoic rocks of the area are often considered to represent the westernmost fragment of the Scythian Platform (e.g. Khain 1977, Săndulescu *vide* Nikishin *et al.* 2001; Natalin & Şengör 2005; Seghedi 2012), deformed by Variscan tectonism and fully amalgamated in one major unit by the end-Middle Jurassic (by Callovian times according to Natalin & Şengör 2005). According to an alternative view these rock complexes represent a slightly tectonized margin of the East European Craton (e.g. Khain 1977; Kruglov & Tsypko 1988; Milanovsky 1996; Nikishin *et al.* 1996, 2001; Mizerski & Stupka 2005; Saintot *et al.* 2006). The Scythian Platform adjoins the East European Craton from the south and is separated from it by a major fault zone, named Scytho-Turanian by Natalin & Şengör (2005) or Sulina-Tarkhankut by Munteanu *et al.* (2011), and interpreted as a Late Variscan through early Alpine trans-regional strike-slip fault. In both, respectively, northern and southern rims of the Fore-Dobrudja Trough this fault and its twin, Sfantu Gheorge Fault, are believed to have continued its originally late Variscan dextral strike-slip transpressional activity throughout the late Permian until the Jurassic (Seghedi 2001; Hippolyte 2002; Natalin & Şengör 2005). Such an intermittently active transpression is believed to have accompanied the Cimmerian folding in the late Jurassic and may have possibly resulted in a compressionally driven (downfolding), instead of extensionally driven (rifting), origin of the end-Permian through Jurassic syndepositional subsidence in the Fore-Dobrudja basin (*cf.* Natalin & Şengör 2005). Across the Scytho-Turanian basement fault the Fore-Dobrudja Trough borders with the Sarmatian segment

(Bogdanova *et al.* 1996) of the East European Craton (Baltica), represented there by the South Ukrainian part of the East European Platform. Sarmatia is considered as one of the three major structural components of Baltica, apart from Fennoscandia and Volgo-Uralia (Gorbatchev & Bogdanova 1993; Bogdanova *et al.* 1996). It is composed of several once independent Archaean domains, that developed at 3.7–2.9, 3.2–3.0 and around 2.7(?) Ga and became juxtaposed with one another across 2.3–2.1 Ga orogenic belts and suture zones (Bogdanova 2005). Within the DOBRE-4 profile, the crust of the East European Craton is composed of a number of Early and Late Archaean and of Early Proterozoic mid-crustal-level igneous and mid- to high-grade metamorphic crystalline massifs (e.g. Schatsky *et al.* 1962; Bogdanov *et al.* 1964; Scherbak 2005, 2008; Galetsky 2007), dismembered with steeply dipping to vertical, most probably deep seated, faults and shear zones into several major crustal blocks (e.g. Sollogub 1982, 1986; Kruglov & Gursky 2004, 2007; Gintov 2005).

At the uppermost crustal level the South Ukrainian Platform is represented by its sedimentary cover composing the South Ukrainian Homocline (Figs 2 and 3), *ca*. 200 km wide (between SP15103 and 108), comprising Ediacaran–Palaeozoic and Triassic–Jurassic sedimentary successions, extending to the NE from the Fore-Dobrudja Trough. The Mesozoic succession of the South Ukrainian Homocline shows much reduced thickness comparing to that in the Fore-Dobrudja Trough. The strata are, in general, very gently (*ca*. 1° on the average) dipping to the SW, although they show slight undulations with wavelengths of tens of kilometres that can be ascribed to tectonic deformation. Rocks of particular systems gradually wedge out toward the NE, to the Ukrainian Shield. They are unconformably covered with subhorizontal, not deformed, Upper Cretaceous, and Oligocene through Neogene deposits (Galetsky 2007), with thickness attaining up to several hundred meters in the SW, but thinning to tens of metres towards the NE and, beyond SP15108, resting directly on top of the crystalline Precambrian basement.

Further to the NE, the DOBRE-4 profile (between SP15109 and 110) enters the Ukrainian Shield, exposing the Precambrian socle on the surface and comprising almost one fourth of the transect's length. The socle mostly crops out in river valleys, emerging from below a thin veneer of Oligocene–Neogene through Quaternary sediments. Along most of its stretch over the shield area, the DOBRE-4 crosses the Ingul 'Megablock' of Early Proterozoic consolidation (between SP15109 and SP15111). This crustal block, of central position within the present-day structure of the Ukrainian Shield, is dissected by a number of deep-seated faults and shear zones of mostly submeridional trends and limited from the east by a N–S elongated, intensely deformed Ingulets-Kryvyi Rih Suture Zone (between SP15111 and SP15112; *cf*. e.g. Gintov 2005; Galetsky 2007; Starostenko *et al.* 2007; Gintov & Mychak 2011a,b). Near its NE end, the DOBRE-4 profile crosses the deep fault/suture zone of Kryvyi Rih-Kremenchug and terminates within the Late Archaean Middle Dnieper crustal block of the Ukrainian Shield.

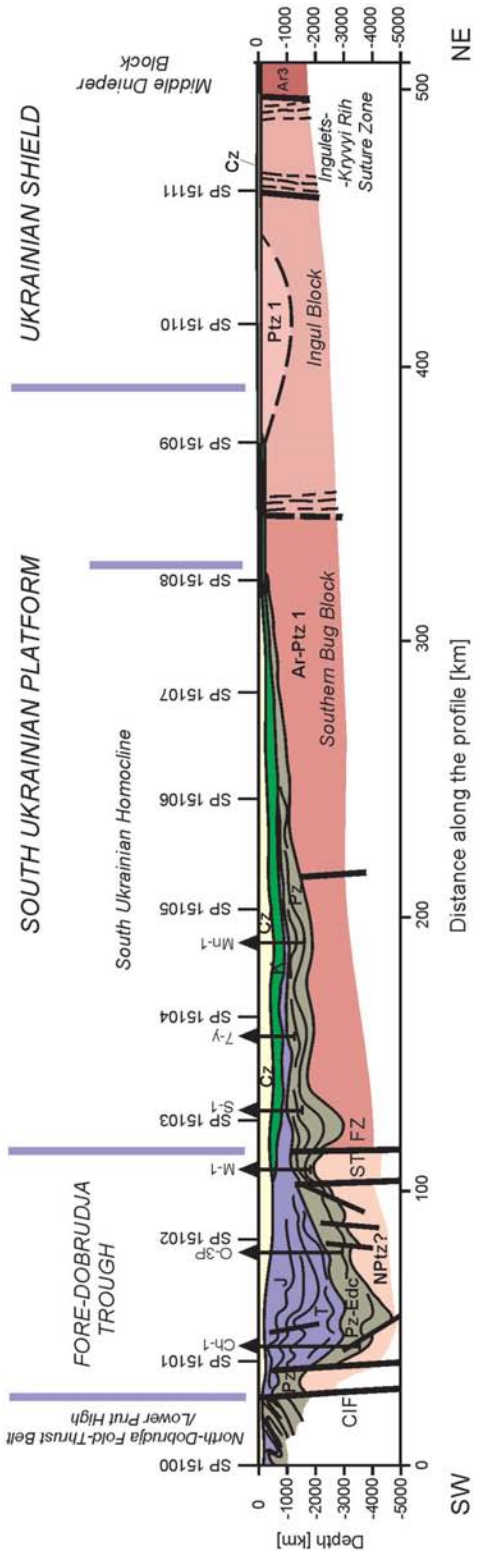

Figure 3. Geological cross-section along the DOBRE-4 profile based on boreholes, reflection seismics and outcrop geology data; vertically 10× exagerrated, much simplified; partly speculative. Age assignments: Ar, Archaean; Ptz, Proterozoic; Edc, Ediacaran; Pz, Palaeozoic; T, Triassic; J, Jurassic; K, Cretaceous; Cz, Cenozoic. Major faults: CIF, Cahul-Ismail Fault; STFZ, Scytho-Turanian Fault Zone. Boreholes: Ch-1, Chervonoarmeyskaya-1 (5.4 km to NW from the profile); O-3P, Orekhovskaya-3P (5.6 km to SE); M-1, Mirnopolskaya-1 (4.2 km to NW); S-1, Saratskaya-1 (5 km to SE); 7-y, 7-U; Mn-1, Mirnenskaya-1.

3 SEISMIC DATA

Several *P*- and *S*-wave phases were correlated in the seismic data and used for later modelling. The seismic record sections show a complex character of the wavefield, particularly the wavefield of the phases reflected from the Moho, reflecting its complicated structure along the profile. All the seismic sections are presented in Fig. 4.

3.1 *P* wave

3.1.1 Refractions

The first *P*-wave arrivals represent the refracted arrivals from the upper crustal sedimentary layers (Psed), the upper/middle crystalline crust (Pg) and the refractions from the upper mantle (Pn). For most of the SPs, the first arrivals can be correlated up to 200–210 km offsets (Pg phase) and to about 400 km (refracted mantle phases).

The Psed phases, representing the refractions in the sedimentary sequences of the uppermost crust, are observed in the southern part of the profile (SP15000–15004) at offsets 0–10 km with apparent velocities between 2.3 and 3 km s^{-1}.

At larger distances (from 10 to 200 km), the Pg phase is observed. Its apparent velocity (5.5–6.2 km s^{-1}) suggests its origin as refractions from the consolidated (crystalline?) basement. The Pg phase in the southern part (SP15100–15104) shows the apparent velocity of 5.5–5.7 km s^{-1} (up to 50 km offset) and 6.3–6.4 km s^{-1} (50–100 km offset). In the north (SP15105–15111) Pg at the offsets up to 50–100 km has the apparent velocity of 5.8–6.1 km s^{-1}, increasing to 6.2–6.3 km s^{-1} in 50–150 to 100–200 km offset range.

The waves propagating in the mantle ($P_{\text{mantle phase}}$) are observed on several SPs for the offsets range about 200–400 km, sometimes with a very high amplitude (e.g. SP15104). Its apparent velocity varies in the range 8–8.3 km s^{-1}. They represent refractions at the Moho (Pn), reflections from the mantle discontinuities (P_1P, P_2P) and possibly also scattered/diffracted arrivals. As the classification of these phases was possible only at the modelling stage, they are discussed later in Section 5.

3.1.2 Reflected arrivals

The scattered crustal reflectivity varies along the profile—in the southern part, at 0–265 km distance, the Pg arrivals and the reflected arrivals are characterized by a strong, incoherent coda of several seconds length, suggesting substantial small-scale reflectivity of the crust (SP15101). In the northern part the Pg arrivals are sharp and short (∼0.6 s) wave trains, followed by a weak coda, sometimes with the amplitudes only slightly higher than the background noise (SP15109, 15111), which suggests that the crust is almost transparent for the seismic waves, except for a few phases from the fragments of larger scale velocity discontinuities. The difference in the coda character can be seen best in the section for SP15105—the Pg and P_MP phases have different characteristics to the south and to the north of the SP. It can be due to the complexity of the sedimentary cover (increasing to the south) or to generally higher deformations of the crust in the southern part.

Coherent reflections form the upper/middle crustal velocity discontinuities are rarely observed. Deeper, reflected waves interpreted as originating from the top of the lower crust are correlated for short (∼20 km) offset intervals for few SPs only—SP15101, 15106 and 15110).

The most striking feature seen in the DOBRE-4 data set are the reflected phases at 7–9 s reduced traveltime and 100–250 km offset range, very coherent and with extremely high amplitudes. In the sections at both ends of the profile they look like typical single P_MP phase (reflection from the Moho boundary). In the other sections, we observe often two separate phases—with slow and fast apparent velocity, crossing each other (e.g. SP15103) or arriving at different reduced time (e.g., SP1507 with shallower Moho reflection at ∼8 s red. time and deeper one at ∼10 s red. time).

The seismic forward modelling showed that these double arrivals represent the reflections from the strongly undulating Moho boundary. The fragments of the traveltime curve with high apparent velocity were generated by the Moho fragments sloping up with increasing offset, while those with slow velocity come from the Moho fragments sloping down. Together, this produces characteristic 'triplication' of the traveltime curve (e.g. Figs 8–10). Usually, these phases are of very good quality, therefore, despite their unusual character, they could be identified with a high confidence.

3.2 *S* wave

The *S* arrivals are of worse quality than the *P* waves. In general, they are of a higher amplitude in the northern part of the profile, probably because of a thinner sedimentary cover. The *S* onsets are often more scattered than the *P* phases, obscured by the P coda and hard to pick consistently. For SP15100 and 15101 in the south, the Sg phase is not visible at all, but S_MS arrivals can be correlated. For other SPs, Sg is of variable quality, while S_MS reflections usually have higher amplitude. In some sections (SP15103), slight increase of the amplitudes at offsets over 200 km suggest a weak upper-mantle refraction (Sn phase).

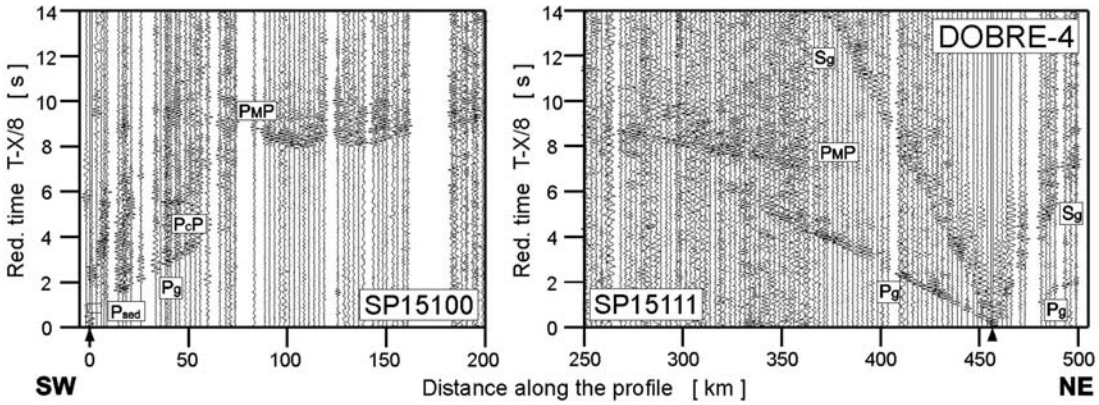

Figure 4. Example of trace-normalized, vertical-component seismic record sections for *P* wave (SP15100–SP15111) filtered by a bandpass filter (2–12 Hz). Pg, seismic refractions from the upper and middle crystalline crust; Pov, overcritical crustal phases; PcP, reflections from the middle crust discontinuities; P_MP, reflected waves from the Moho boundary; Pn, refractions from the sub-Moho upper mantle; $P_{\text{mantle}}P$, *P*-wave phases from the upper mantle. The reduction velocity is 8.0 km s^{-1}.

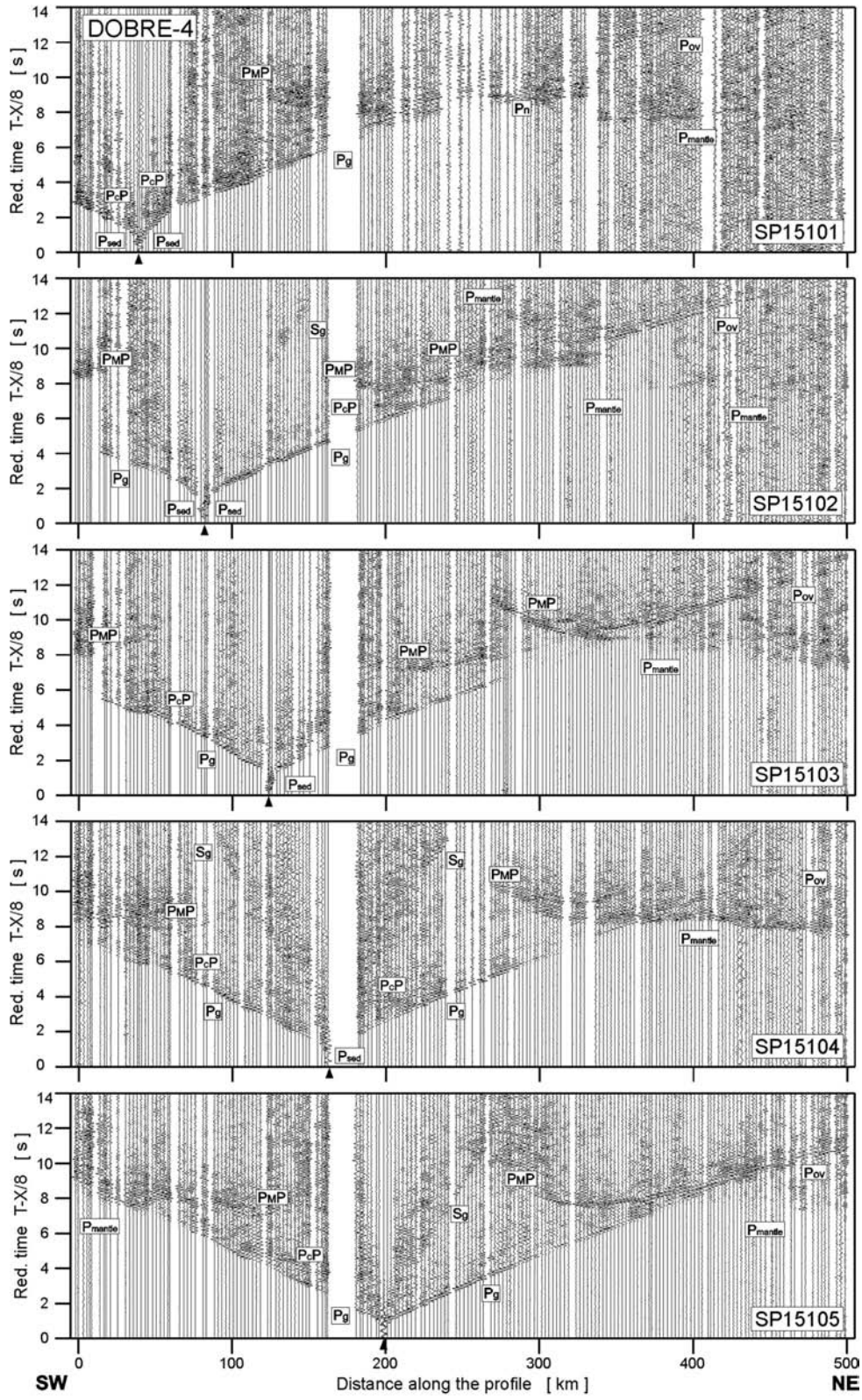

Figure 4. (*Continued.*)

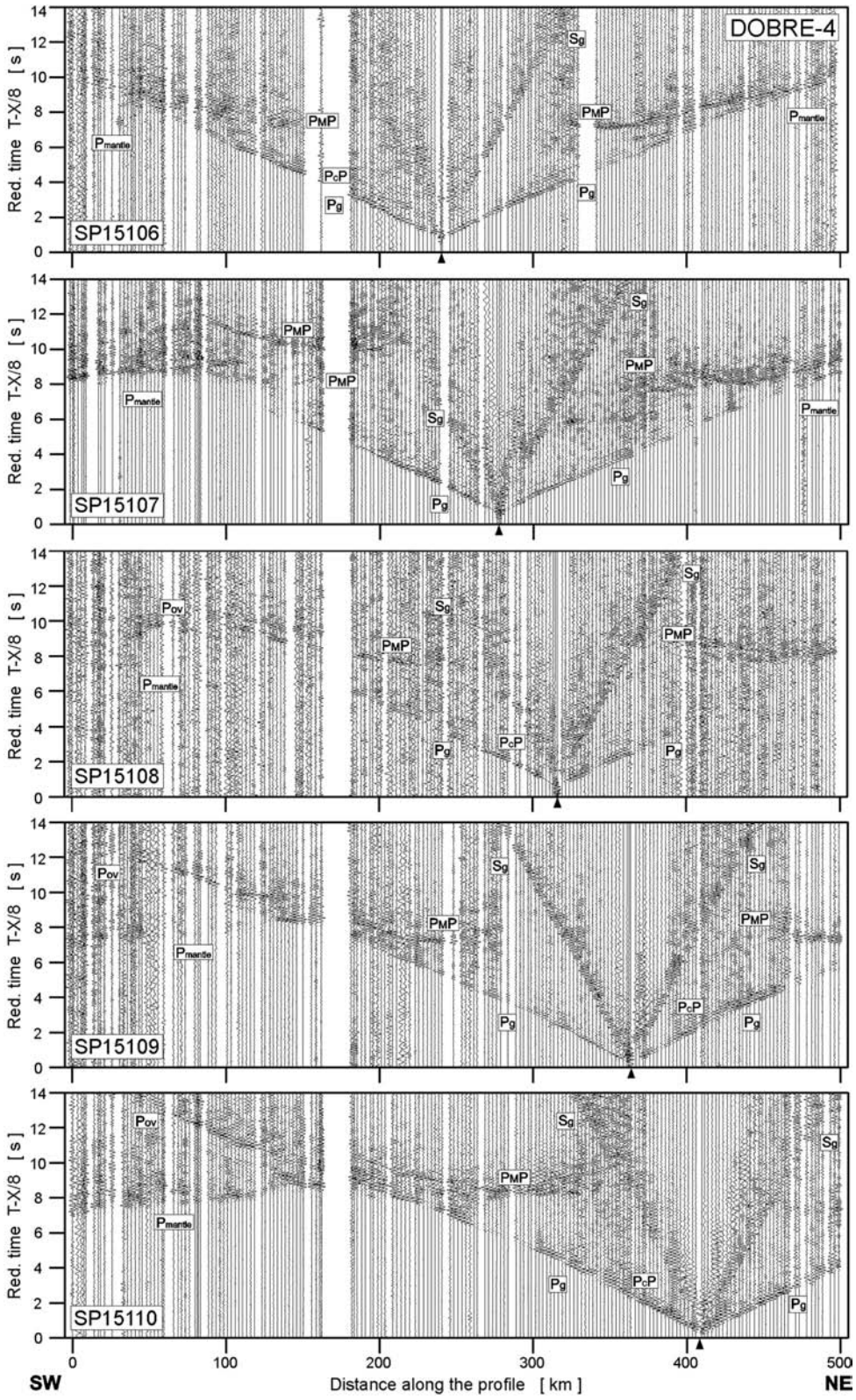

Figure 4. (*Continued.*)

4 SEISMIC MODELLING METHODS

Two methods were used for the modelling of the seismic data. First, ray tracing trial-and-error modelling was performed. Next, analysis of the amplitudes of the recorded phases was applied using finite difference (FD), full waveform calculation.

4.1 Ray tracing modelling

The trial-and-error forward modelling was done using the SEIS83 package (Červený & Pšenčík 1984) with the graphical interface model (Komminaho 1998) and ZPLOT (Zelt 1994). The algorithm uses the ray method for tracing of the ray paths and calculation of the traveltimes as well as the synthetic seismograms in the high-frequency approximation. The model consists of layers with seismic velocity parametrized on an irregular rectangular grid and interpolated by bicubic splines. Velocity discontinuities are allowed across the layer boundaries. The geological and geophysical data provided by boreholes and nearby seismic studies (Fig. 5, second diagram) were used to prepare an initial model of the velocity distribution in the uppermost crust. The solution was sought iteratively: the traveltimes, calculated for the current V_p model, were compared with the observed traveltimes. Based on traveltime differences, the model was corrected in order to minimize the misfit. The modelling also involved the calculation of synthetic seismograms and qualitative comparison of amplitudes of synthetic and observed data. This provided additional constraints on the velocity gradients and contrasts at the discontinuities.

Usually, the modelling algorithms based on ray theory are enough to calculate the traveltime curves and to produce the velocity model. For the DOBRE-4 profile, this approach worked very well for the crustal model, However the topography of the Moho discontinuity (e.g. ∼13 km difference of the Moho depth over ∼50 km horizontal distance) prevented calculation of theoretical traveltimes of the mantle refracted phases (strongly dipping interfaces, for example, deep synforms, produce the shadow zones in the geometrical ray approximation). Therefore, for modelling of the upper-mantle velocity distribution, two concurrent approaches were applied. The first one, was based only on the ray theoretical algorithm The velocity discontinuities were introduced in the mantle in order to change the ray paths by reflection or refraction, to allow the rays to propagate into the shadowed zones, with a path of a shape similar to a refracted phase, thus simulating a Pn-like arrivals (Fig. 6, third diagram).

The other approach used the full waveform FD modelling to overcome the limitations of the ray method. For working purposes, the MPM program (Hansen & Jacobsen 2002) was used, while final versions of synthetic sections were calculated using the Tesseral 2-D package (Kostyukevich *et al.* 2000). The synthetic seismograms calculated in this way showed mantle arrivals even in previously shadowed zones, which allowed for the comparison of their traveltimes with the experimental ones. This resulted with simpler mantle structure with less discontinuities and less velocity contrasts (Fig. 6, bottom diagram) and, at the stage of phases correlation, helped greatly to correctly identify the observed mantle phases from the regions with complicated Moho topography.

4.2 Full waveform modelling

The full wave modelled synthetic sections were calculated based on the finite-difference method using Tesseral 2-D package (Kostyukevich *et al.* 2000). The final ray tracing velocity model was expressed as a grid with 500 m spacings horizontally and 100 m vertically. The grid of *S*-wave velocities was obtained from values of V_p/V_s ratio for each layer. For those layers where the quality of *S*-wave record sections was good or adequate, the modelled values of the V_p/V_s ratio were used. For other layers the default values of V_p/V_s ratio were used. Both *P*- and *S*-wave grids formed an input model for full wave modelling. As well as for ray tracing modelling, the surface topography was also taken into account.

The observation scheme included 206 receivers with the 2500 m interval. The dominant frequency of the source impulse was 10 Hz and this is the maximum frequency with which it was possible to calculate a model of such size in reasonable time, using the available computation resources. Due to large volume of input data, the computations were performed on a grid of computers using parallel computation algorithms (Kolomiyets & Kharchenko 2008).

Full waveform modelling allows simulation of the wave propagation through the modelled structure such that all wave transformations (reflection, refraction, reverberations, etc.) on the main boundaries in the model can be visualised through time.

The comparison of the calculated full-wave synthetic sections with seismic record sections for both the models are presented in Figs 6–11.

5 *P*-WAVE VELOCITY MODEL

The forward modelling of 13 *P*- and *S*-wave record sections produced a seismic *P*-wave velocity model and a distribution of the V_p/V_s ratio beneath the 505-km-long DOBRE-4 profile. In the southwestern part of the profile our starting model is based on the data collected from six 1.5 to 3.5 km deep boreholes located within 5.6 km from the profile. The models are presented in Fig. 5. Examples of the 2-D ray tracing modelling of the crust for different parts of the profile are shown in Figs 6–12.

The ray tracing modelling helped us to identify the upper-mantle phases on seismic sections. The Pn phase is usually observed as first arrival. Sometimes, due to large differences in the Moho depth and the complex geometry of the Moho (e.g. SP15103 and SP15105) Pn waves are visible as strong later pulses after first arrivals, with apparent velocities lower than 8 km s^{-1} (Figs 8 and 9). We found out that the Pn phase from the uppermost mantle sometimes is not observed as first arrival probably because of too small amplitudes. Then, as for example, in SP15103, rays penetrating deeper into the mantle, interpreted as reflected, are visible on the section as first arrivals.

5.1 Crustal layers

In the 0.5–4.2-km-thick sedimentary layer the *P*-wave velocity varies generally between 2.3 and 5.45 km s^{-1}. The deepest, *ca.* 2–3 km deep and 40 km wide sedimentary trough with *P*-wave velocities 2.3, 2.7, 3.75 and 4.75 km s^{-1}, and $V_p/V_s = 1.55$ is observed below the Fore-Dobrudja Trough. These *ca.* 1-km-thick sedimentary layers extend to southwest approximately up to a distance of 360 km. Below these layers, northwest from the deepest sedimentary trough, a 1–2-km-thick layer with *P*-wave velocities of 5.1–5.15 km s^{-1} and V_p/V_s of 1.52–1.55 is found. More to the northwest, below the Ukrainian Shield, the same layer with slightly larger velocity, *ca.* 5.45 km s^{-1}, and with $V_p/V_s = 1.71$, shallows almost to the surface. Its thickness varies from *ca.* 1.0 to 1.3 km below the Ingul block to 0.25 km below the Ingulets–Kryvyi Rih suture zone and the middle Dnieper block. The crystalline rocks

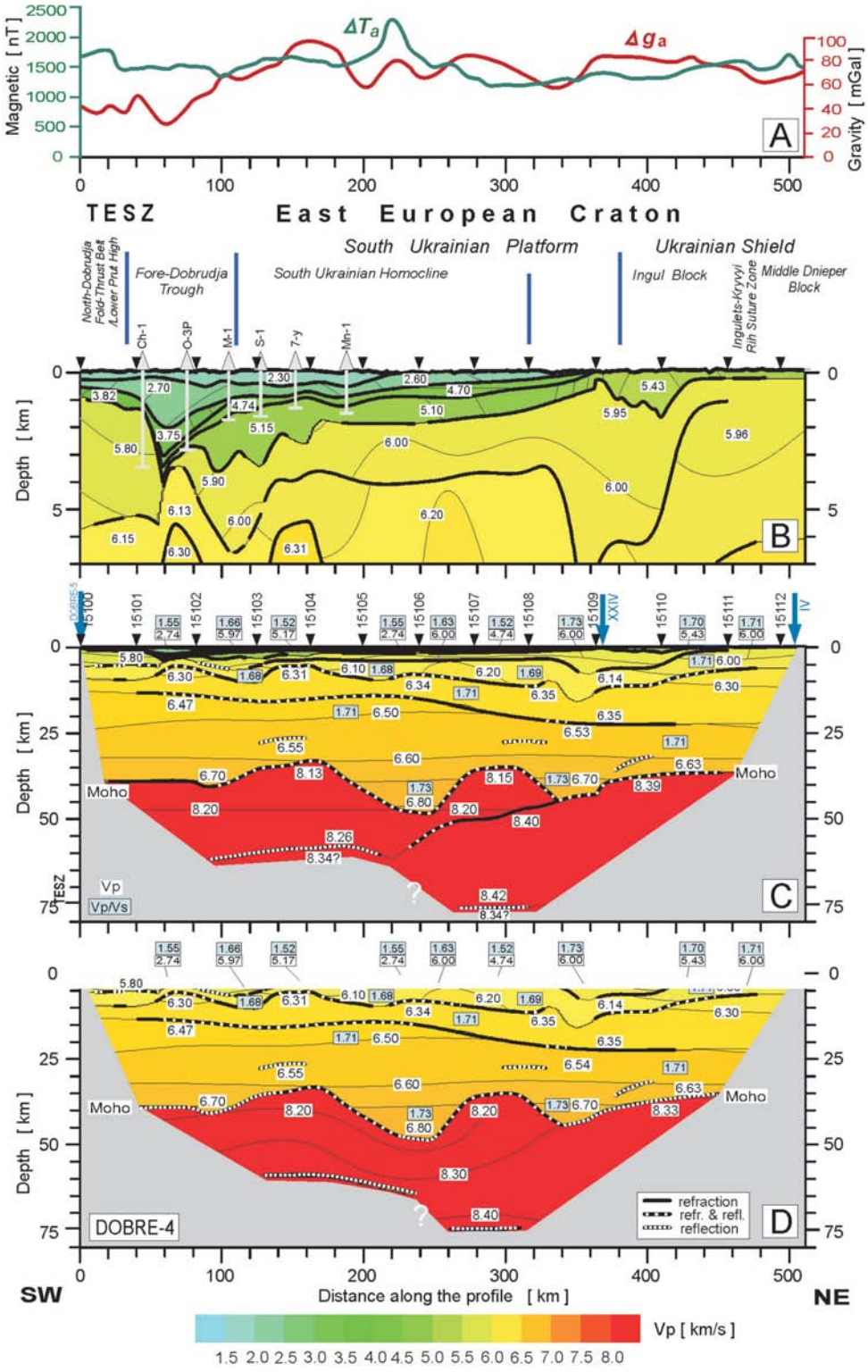

Figure 5. 2-D models of seismic *P*-wave velocity in the crust and uppermost mantle along DOBRE-4 profile, complemented with gravity and magnetic data. (a) Bouguer gravity and total magnetic field anomalies (after Khomenko 1987; Kruglov 2001), (b) *P*-wave velocity model of the uppermost crust, (c) *P*-wave velocity model of the crust and upper mantle derived from forward ray tracing modelling, using SEIS83 package (Červený & Pšenčík 1984), (d) *P*-wave velocity model of the upper mantle derived from full waveform modelling using MPM package (Hansen & Jacobsen 2002), whereas the same ray tracing-derived model as in (d) is used for the crust. Thick, black lines represent major velocity discontinuities (interfaces) constrained by reflected or/and refracted arrivals of *P* waves. Thin lines are velocity contours with values in km s^{-1} shown in white boxes. Position of major crustal tectonic units is indicated above (b). Arrows show positions of shot points. Blue arrows are at intersections with other seismic profiles. Other abbreviations same as for Fig. 3. Vertical exaggeration is 6.7:1 in (b) and 2.4:1 in (c) and (d). V_p/V_s values are displayed in blue rectangles.

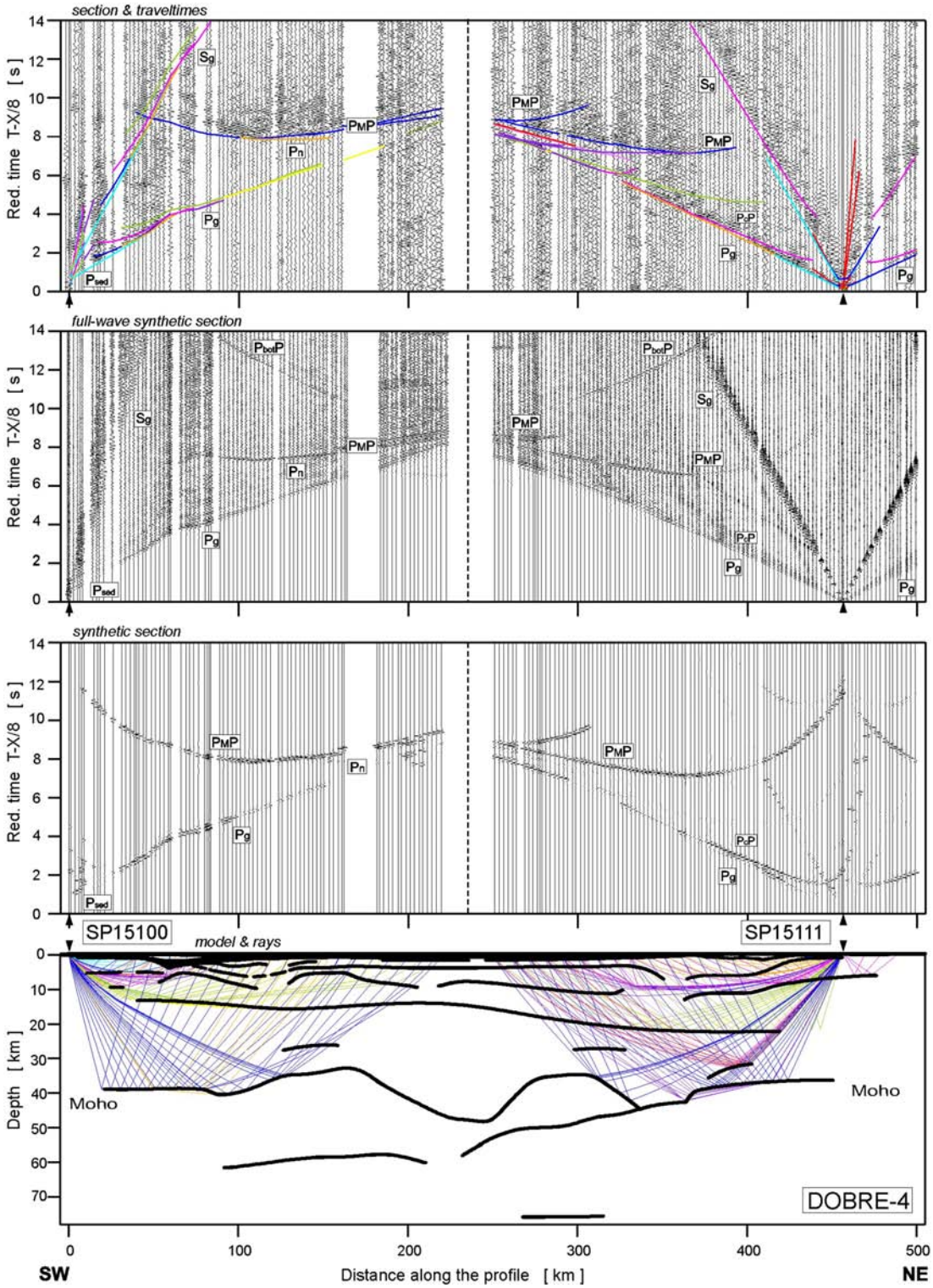

Figure 6. Example of seismic modelling for SP15100 and SP15111; seismic record sections (amplitude-normalized vertical component) of *P* wave with theoretical traveltimes calculated using the SEIS83 ray tracing technique. *P*-wave data have been filtered using the bandpass filter of 2–12 Hz and displayed using the reduction velocity of 8.0 km s^{-1}. Full-wave synthetic seismograms (second diagram) using TESSERAL program were calculated for the bottom model presented in Fig. 5. Synthetic seismograms (third diagram) and ray diagram of selected rays using the SEIS83 (bottom diagram) were calculated for the model presented in third diagram of Fig. 5. $P_{bot}P$, artificial *P*-wave phases from the bottom of the model. Other abbreviations are as in Figs 4 and 5.

are divided into four layers. The *P*-wave velocities of the three uppermost layers are 5.8–6.0, 6.1–6.2 and 6.3–6.35 km s^{-1} and values of V_p/V_s ratios are 1.66–1.71, 1.68–1.71 and 1.71, respectively. The highest values of V_p/V_s ratio are observed, similar as for subsurface layer, at the Ukrainian Shield and directly south of it. Two boundaries separating three upper crystalline layers from one another are strongly undulating. The total thickness of this part of the crust varies from approximately 12 km near the southwestern

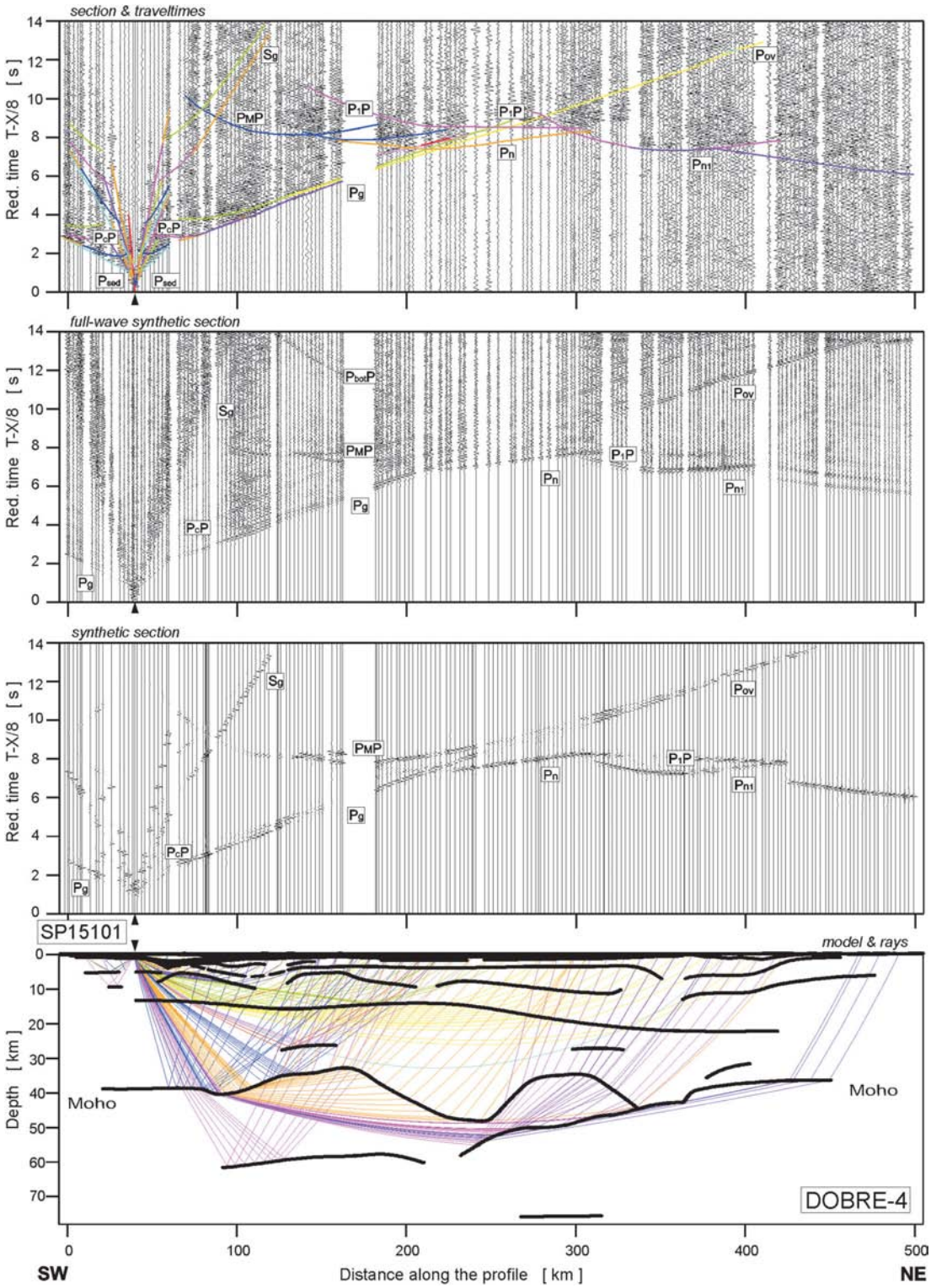

Figure 7. Example of seismic modelling for SP15101; Seismic record sections (amplitude-normalized vertical component) of *P* wave with theoretical traveltimes calculated using the SEIS83 ray tracing technique. *P*-wave data have been filtered using the bandpass filter of 2–12 Hz and displayed using the reduction velocity of 8.0 km s^{-1}. Full-wave synthetic seismograms using TESSERAL program (second diagram). Synthetic seismograms (third diagram) and ray diagram of selected rays using the SEIS83 (bottom diagram). All examples were calculated for the model presented in third diagram of Fig. 5. Other abbreviations are as in Fig. 6.

end of the profile up to 20 km near northeastern end of the profile. The fourth layer is 15–35 km thick with *P*-wave velocities of ∼6.45 and ∼6.8 km s^{-1} reaching the Moho boundary. We observe sporadic reflections from the floating reflectors within this layer (Fig. 5) at the depths of 30–35 km. These reflectors separate the layer into upper part with $V_p/V_s = 1.71$ and lower part, with $V_p/V_s = 1.73$. Clear overcritical reflections, observed on several record sections, allowed us to control velocities up to depths of 35 km.

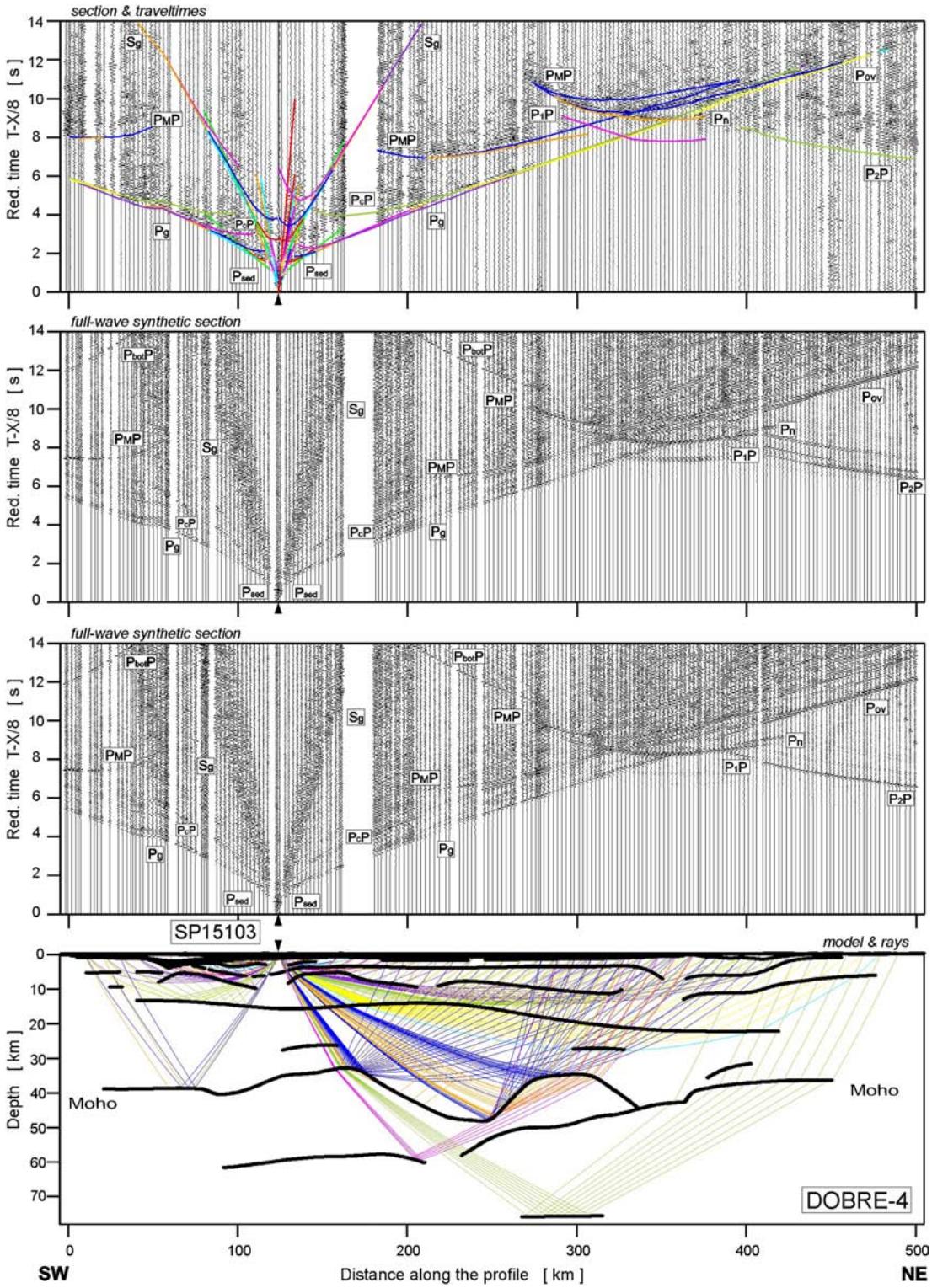

Figure 8. Example of seismic modelling for SP15103; Seismic record sections (amplitude-normalized vertical component) of *P* wave with theoretical traveltimes calculated using the SEIS83 ray tracing technique. *P*-wave data have been filtered using the bandpass filter of 2–12 Hz and displayed using the reduction velocity of 8.0 km s^{-1}. Full-wave synthetic seismograms using TESSERAL program for the bottom model presented in Fig. 5 (second diagram), and for the model presented in third diagram of Fig. 5 (third diagram). Ray diagram of selected rays using the SEIS83 (bottom diagram). Other abbreviations are as in Fig. 6.

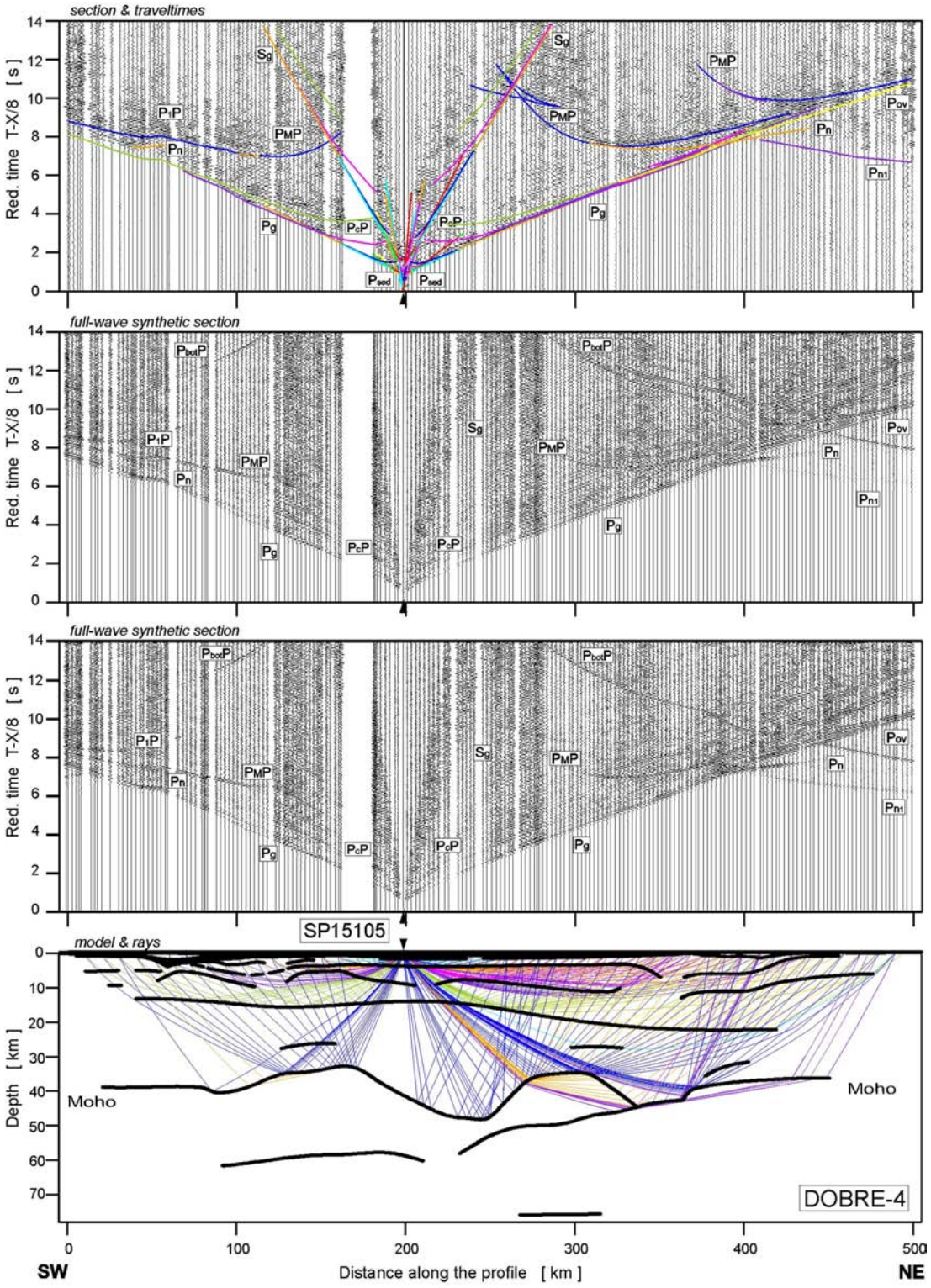

Figure 9. Example of seismic modelling for SP15105; Seismic record sections (amplitude-normalized vertical component) of *P* wave with theoretical traveltimes calculated using the SEIS83 ray tracing technique. *P*-wave data have been filtered using the bandpass filter of 2–12 Hz and displayed using the reduction velocity of 8.0 km s^{-1}. Full-wave synthetic seismograms using TESSERAL program for the bottom model presented in Fig. 5 (second diagram), and for the model presented in third diagram of Fig. 5 (third diagram). Ray diagram of selected rays using the SEIS83 (bottom diagram). Other abbreviations are as in Fig. 6.

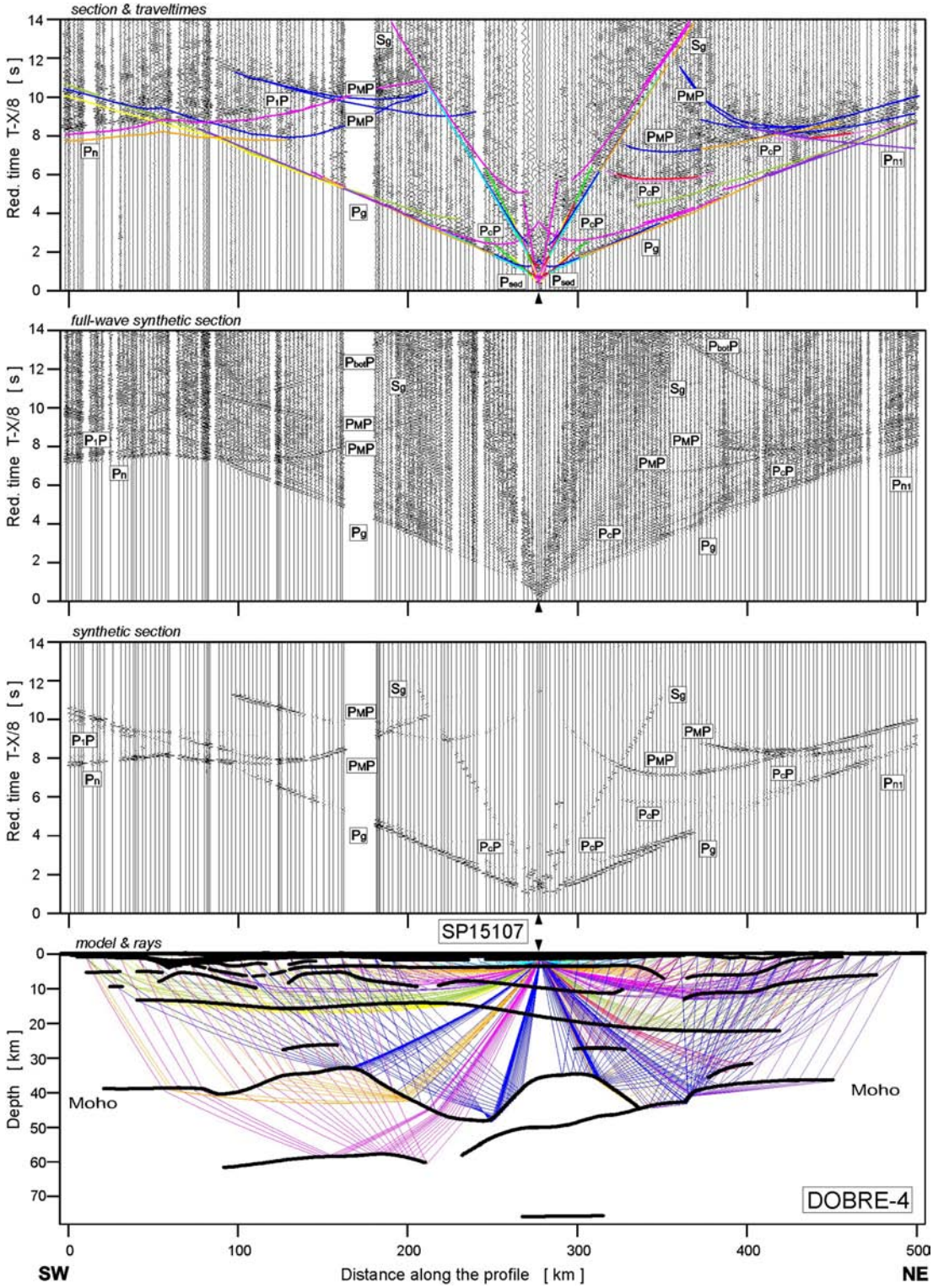

Figure 10. Example of seismic modelling for SP15107; Seismic record sections (amplitude-normalized vertical component) of *P* wave with theoretical traveltimes calculated using the SEIS83 ray tracing technique. *P*-wave data have been filtered using the bandpass filter of 2–12 Hz and displayed using the reduction velocity of 8.0 km s^{-1}. Full-wave synthetic seismograms using TESSERAL program (second diagram). Synthetic seismograms (third diagram) and ray diagram of selected rays using the SEIS83 (bottom diagram). All examples were calculated for the model presented in third diagram of Fig. 5. Other abbreviations are as in Fig. 6.

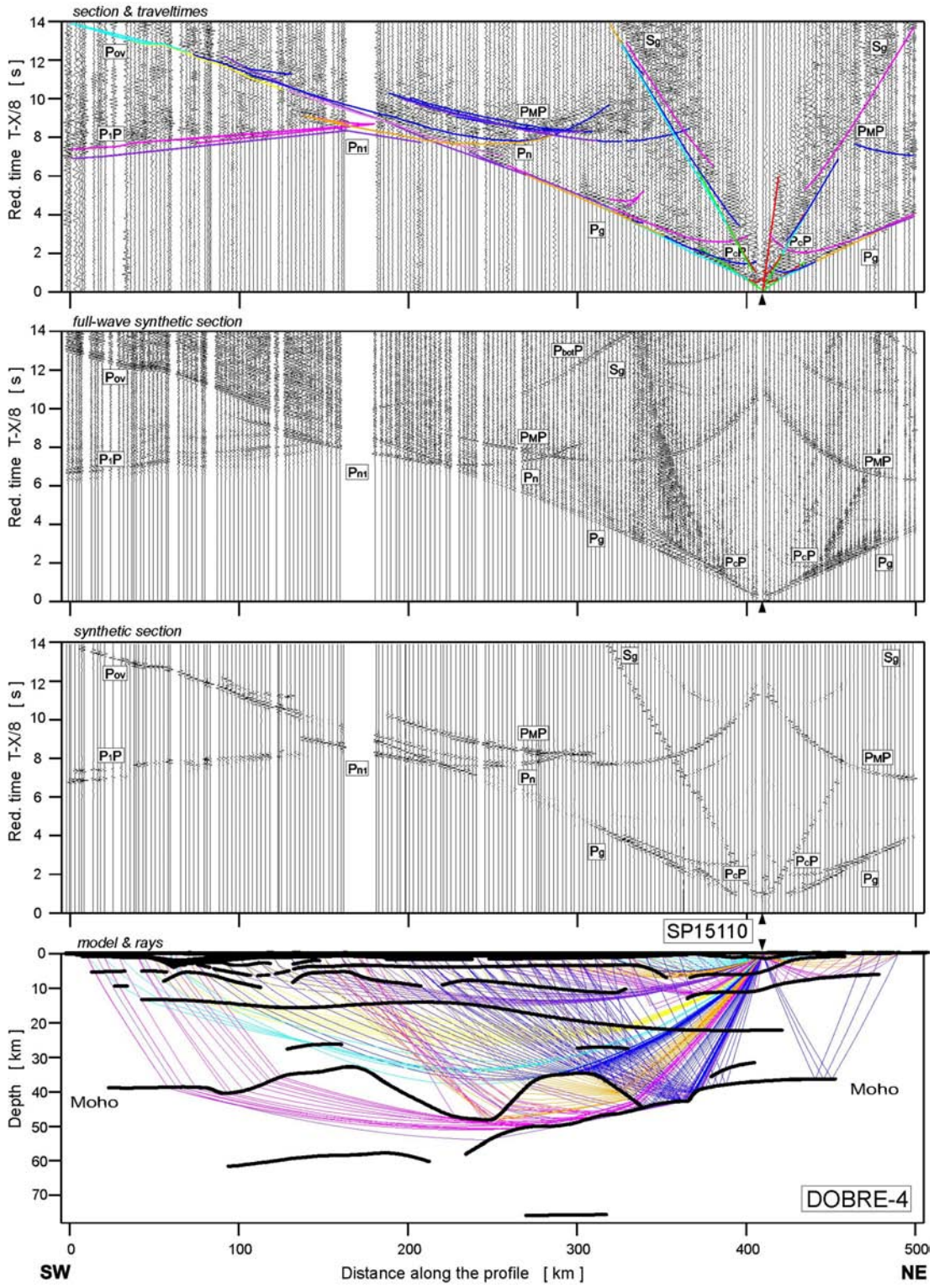

Figure 11. Example of seismic modelling for SP15110; seismic record sections (amplitude-normalized vertical component) of *P* wave with theoretical traveltimes calculated using the SEIS83 ray tracing technique. *P*-wave data have been filtered using the bandpass filter of 2–12 Hz and displayed using the reduction velocity of 8.0 km s^{-1}. Full-wave synthetic seismograms (second diagram) using TESSERAL program were calculated for the bottom model presented in Fig. 5. Synthetic seismograms (third diagram) and ray diagram of selected rays using the SEIS83 (bottom diagram) were calculated for the model presented in third diagram of Fig. 5. Other abbreviations are as in Fig. 6.

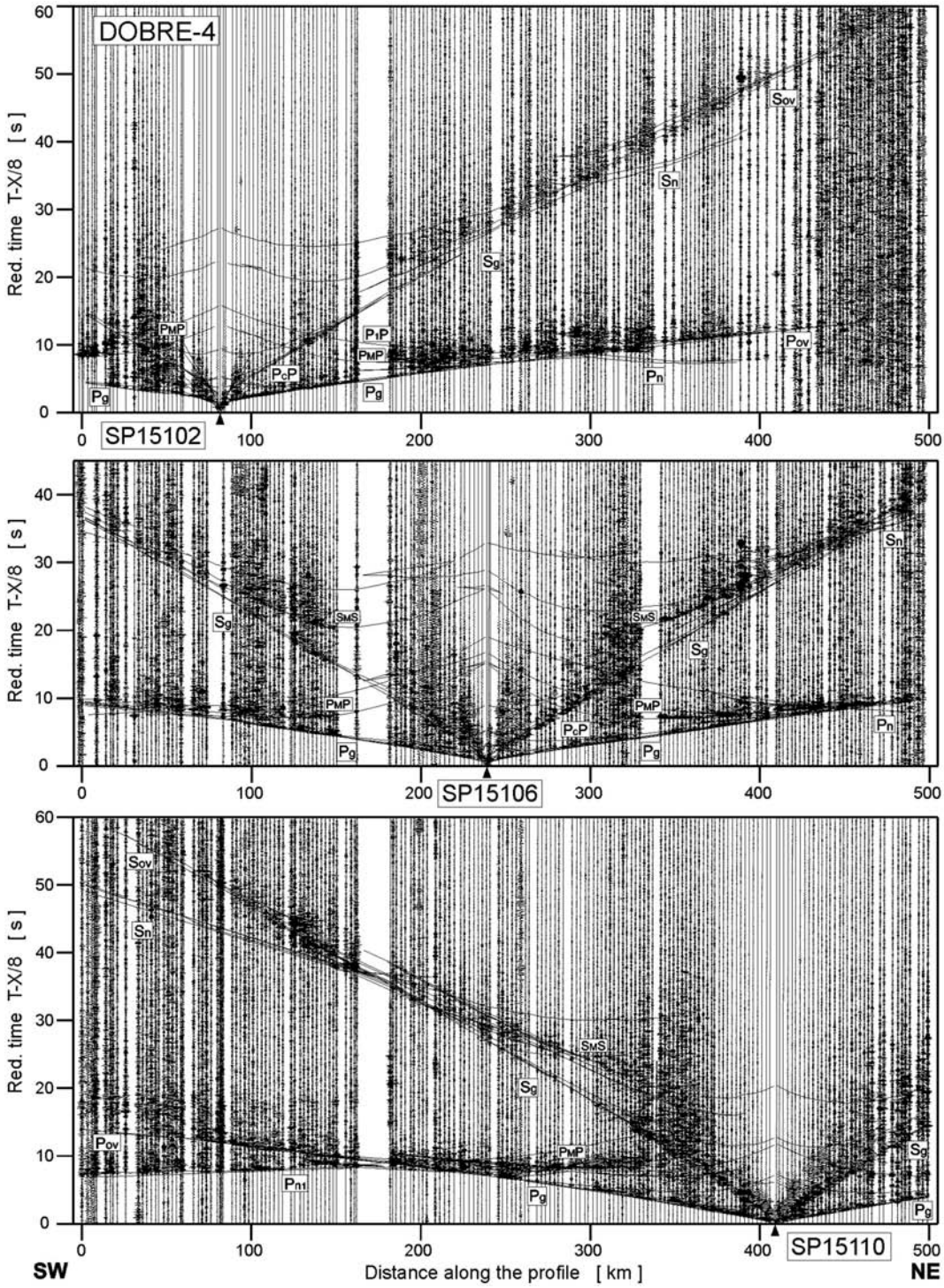

Figure 12 Examples of trace-normalized, vertical-component, common seismic record sections for *P* and *S* waves (SP151002, SP151006 and SP151010) filtered by a bandpass filter (1–8 Hz).

5.2 Moho boundary and upper mantle

5.2.1 Classification of the mantle phases

The trial-and-error ray tracing modelling showed that some parts of the mantle phases in the first arrivals represent the refraction at the Moho discontinuity (Pn phase), while other parts (e.g. SP15101 offsets 320–490 km) seem to be generated differently, as they are observed at offsets where in geometrical optics (ray method) approach a shadow zone for refractions occurs, due to large changes of the Moho depth. Therefore, it is difficult to model this phases using the ray method, since it relies on comparing of the computed and observed traveltimes. In order to overcome the limitations of the ray method, full waveform forward modelling of the mantle phases was carried out. Its results are presented in the bottom diagram of Fig. 7.

In the synthetic sections calculated in full waveform approach, the mantle phases extend also over the 'geometrical' shadow zones, similarly as in the real data. We suggest that these phases could have been generated as diffractions at the Moho boundary or as waves scattered by random mantle heterogeneities, located close to the path of the refracted rays. Both mechanisms involve radiating of seismic energy into the shadow zone, producing the arrivals with traveltime close to the Pn phase, and of slightly smaller amplitude.

Additionally, waves reflected from the upper-mantle discontinuities were recorded, usually with an amplitude exceeding the Pn amplitude (SP15107). On some record sections at offsets >200 km (e.g. SP15103), first observed arrivals are clearly visible at ∼7.5 s reduced traveltime. Their character and apparent velocity (over 8 km s^{-1}) suggest that they may represent the Pn phase. However, later comparison with ray tracing traveltimes and full-wave synthetic sections proved that even if they are seen as (apparently) first arrivals, they are reflected from a mantle discontinuity. A strong Moho topography creates 'shadow zones' for the Pn wave. This either prevents its propagation or decreases its amplitude below the noise level, making it invisible in the real data, even if it is observed as a very weak phase in the noise-free synthetic section, *ca*. 0.7 s earlier than stronger, clearly observed arrival (Fig. 8). These stronger, first observed arrivals can be explained as mantle reflections.

The model shows large variations in the Moho depth. Below the TESZ (to a distance of 80 km from the beginning of the profile), the Moho is nearly flat at a depth of 39 km. In the next segment of the profile, to a distance *ca*. 360 km mainly below the South Ukrainian Homocline and partly below the Ukrainian slope, the Moho has two huge undulations. The largest depth change in Moho boundary is from 32 km at a distance of 165 km, down to 48 km at a distance of 250 km. At a distance of 300 km, the Moho boundary rises again to depth of 35 km. Next, to the northeast, there is a small Moho depression (depth 44 km) below the southern margin of the Ukranian Shield. Towards the end of the profile, below the Ukrainian Shield, the Moho is slightly shallowing to a depth of 36 km (at km 450).

The sub-Moho velocities are *ca*. 8.15 km s^{-1} for the southwestern and centrals part of the profile, while beneath the Ukrainian Shield (from *ca*. 330 km on, they are higher than 8.3 km s^{-1}. A significant feature in the upper-mantle structure is a southwest dipping mantle interface, from the depth of 50 km (at distance 340 km) to 60 km (at distance 240 km), in ray tracing model. It separates areas of relatively lower (8.15–8.25 km s^{-1}) and higher (8.3–8.4 km s^{-1}) velocities. An alternative solution is presented in the bottom diagram of Fig. 5 where the interface is replaced by a zone with gradually changing velocities. This solution was used for FD-modelling. The crustal models used in ray tracing modelling and in FD modelling were almost the same. For technical reasons there is a small difference in the Moho boundary at distance 360 km.

The highest (∼8.4 km s^{-1}) upper-mantle velocities are observed at distances of 260–315 km at the depth of 70 km. Beneath the EEC, some subhorizontal reflectors were visible in the upper mantle, about 20–30 km below the Moho at the depths of ∼60 km and 75 km.

5.3 Resolution analysis for models obtained by ray tracing

Using modern GPS techniques, the shot times and locations for shots and receivers were measured very precisely, in the order of 1 ms and tens of metres, respectively. Such errors are insignificant in a crustal-scale experiment. Uncertainties of velocity and depth in the model obtained using the ray tracing technique result first of all from the uncertainties of subjectively picked traveltimes, which is of the order of 0.1 s. However, the accuracy increases with increasing quality and amount of data (number of shots and receivers, effectiveness of sources, signal-to-noise ratio, check of reciprocity of the traveltime branches, ray coverage in the model).

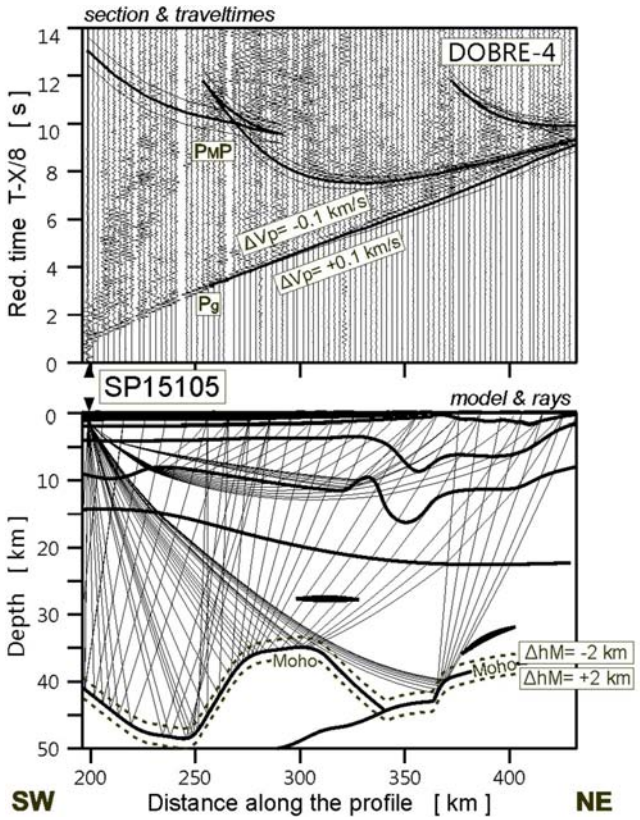

Figure 13. Seismic record section for the shot point 15105 with some Pg and P_MP traveltimes calculated with perturbed, from the final model, *P*-wave velocity in one crustal layer (Pg) in the range of ±0.1 km s^{-1} as well as separately the Moho depth (P_MP) in the range of ±2 km. Reduction velocity is 8 km s^{-1}.

Good quality of analysed data allowed to construct a velocity model that fitted the observed (experimental) traveltimes for both refracted and reflected waves with good accuracy. Several modelling tests were performed. An example is shown in Fig. 13. The *P*-wave velocity in one crustal layer was perturbed, relatively to the final model, by ±0.1 km s^{-1}. Independently, the Moho depth was perturbed by ±2 km. It is clearly visible that accuracy of our model is better than these values. Similar tests were performed by, for example, Janik *et al.* (2002), Grad *et al.* (2003b, 2006a,b), Środa *et al.* (2006), Grad *et al.* (2008) and Janik *et al.* (2009). Diagrams showing theoretical and observed traveltimes for all the phases along the profile, ray coverage and traveltime residuals from forward modelling are shown in Fig. 14. The rms values are acceptable, being 0.36 for sediments, 0.21 for the crust and 0.17 for P_MP and 0.31 for Pn phases, and 0.74 for all the upper-mantle phases. The rms value for refracted phases in the crust is 0.11 while for reflections it is 0.30. The overall rms value for 3880 picks is 0.37. It means that calculated traveltimes for refracted phases in the crust fit better experimental arrival times than these for reflected phases. Calculated traveltimes for Moho reflections are better modelled than average intracrustal reflection traveltimes.

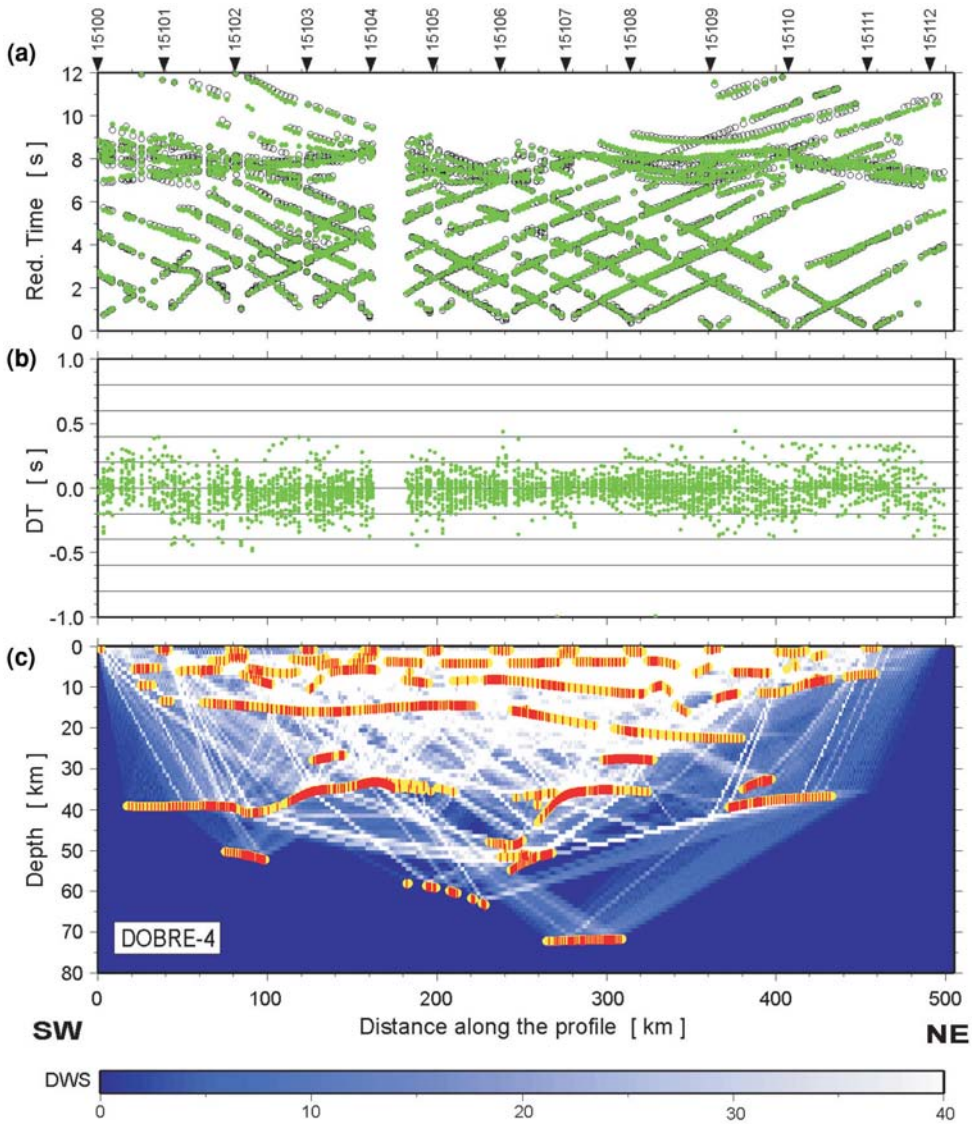

Figure 14. Diagrams showing theoretical and observed traveltimes (a), traveltime residuals (b) and ray coverage (c) from forward modelling along profile DOBRE-4. Green points, refracted arrivals; red points, reflections; black circles, theoretical traveltimes. Yellow lines, fragments of discontinuities constrained by reflected phases. The red points plotted along the interfaces mark the bottoming points of the modelled reflected phases (every third point is plotted) and their density is a measure of the positioning accuracy of the reflectors. DWS, derivative weight sum. Reduction velocity is 8 km s^{-1}.

6 COMPARISON WITH RESULTS OF THE PREVIOUS STUDIES

The investigated area has been previously extensively studied by various geophysical methods. The Geotraverse VIII was located close and subparallel to the DOBRE-4 profile. It was carried out using the wide-angle (Chekunov 1988) and CDP (Borodulin & Baysarovich 1992) seismic techniques. The U.S. structures were studied also by Geotraverses IV and VI (Sollogub *et al.* 1988).

In the southern part of the Geotraverse VIII, the sediments thickness reaches 1–2 km and decreases to the NE, similarly as in the DOBRE-4 model. In the deeper layers, the velocities down to *ca.* 12 km in the SW and to *ca.* 20 km in the NE (corresponding to the upper crust in the presented model) are in the range of 6.0–6.4 km s^{-1}—similarly to the velocities observed in the DOBRE-4 model (6.0–6.35 km s^{-1}). The middle/lower crustal velocities are also similar along both profiles (6.5–6.8 km s^{-1}), except in the ∼120 km wide area between SP15104 and 15107 (corresponding to the Southern Bug Block below the South Ukrainian Homocline), where the Geotraverse VIII model documents substantially higher velocities—6.6 to 7.5 km s^{-1}, compared to 6.5–6.8 km s^{-1} along the DOBRE-4. This high-velocity body, outlined by diffraction points and reflecting boundaries, was interpreted as a mafic intrusion. However, in the modelling, reflected phases and the method of effective parameters (e.g. Egorkin 1966; Grad 1983) were used. Under the DSS conditions, the value of the effective velocity may exceed the value of the mean velocity even by 10–15 per cent. The effective depth determined from the reflected wave traveltime is also greater than the true depth of the reflecting boundary. The difference increases with distance from the source, and under the DSS conditions, it may exceed 20–30 per cent (Grad 1983; Janik *et al.* 2009). Outside the area with lower crustal high velocities, the depth to the Moho discontinuity is only slightly higher than along the DOBRE-4: 35–45 km versus 33–44 km. Beneath the high velocity area, the Moho depth calculated at Geotraverse VIII (58 km) is substantially higher than for the DOBRE-4 (48 km), but

generally the shapes of the Moho boundary are similar. A similar depth, *ca*. 58 km and high velocities in the lower crust were detected to the NE from the DOBRE-4 profile along Geotraverse VIII at the intersection with the P-K profile (Chekunov *et al.* 1992). Assuming similar traveltimes of the P_MP phase in both experiments, this difference in the Moho depth reflects the large difference in the seismic velocity of the overlying lower crust in both models, due to the well-known velocity–depth trade-off.

The CDP profile along Geotraverse VIII provided an image of crustal and upper-mantle reflectors (Borodulin & Baysarovich 1992). In the upper crust to depths of 10–15 km, reflections from inclined horizons dominate, while horizontal events prevail in the lower crust. In the CDP section, the crust-mantle boundary is not observed as a sharp horizon, but its location can be inferred at the bottom of the reflective zone along subhorizontal events, 2–4 km long, in the time range of 9–12 s. The wide-angle Moho coincides largely with the lower part of this zone, However, in some areas, it correlates rather with the middle part or the top of the zone, apparently representing the crust-mantle transition. In the uppermost mantle, generally showing low reflectivity, short, dipping events, sometimes penetrating into the crust, can be traced. They are interpreted as possible faults/shear zones accommodating tectonic deformation. Deeper, horizontal reflectors are observed in 15–20 s interval beneath the Kryvyi Rih block and 25–27 s near Odessa.

Materials collected earlier along the Geotraverses IV and XXIV were reinterpreted using ray tracing and presented by Grad & Tripolsky (1995) and Grad *et al.* (2006b) (by mistake they numbered the Geotraverse IV as the VIII). Similar Moho synformal deflections as those observed between the SP15102 and SP15109 on the DOBRE-4 profile were earlier modelled along the Geotraverse IV beneath the Ukrainian shield. Grad & Tripolsky (1995) modelled velocities 6.4–7.25 km s^{-1} and 41–55 km Moho depth for the Podole block, and 6.3–7.0 km s^{-1} and 38–50 km for the Kirovograd block, respectively. The Geotraverse XXIV at the intersection with the DOBRE-4 profile has a similar depth of the Moho (*ca*. 37 km) and of the velocities above and below the Moho (6.8 and 8.1 km s^{-1}, respectively). Along both transects, similarly as for the DOBRE-4, the structure of the middle and lower crust is practically transparent.

In addition, numerous seismic soundings were performed in the Kryvyi Rih region to study the Moho boundary and to construct a 3-D crustal model (Sharov 2004; Starostenko *et al.* 2007) in the area of Kryvyi Rih ultradeep borehole (Chekunov *et al.* 1989).

Along a fragment of the VRANCEA2001 seismic line (Hauser *et al.* 2007) located in the North Dobrudja Fold-Thrust Belt some 30 km from the SW end of the DOBRE-4 profile, the Moho boundary was modelled at a depth of 44 km, that is 6 km deeper than in this study. As the VRANCEA2001 model assumes higher lower crustal velocities (6.7–7.1 km s^{-1}), the difference may be due to the velocity depth trade-off.

7 TECTONIC INTERPRETATION

7.1 Upper lithospheric structure along DOBRE-4

The obtained 2-D model of seismic *P*-wave velocity (Fig. 5) shows a number of peculiarities, when compared to models from other seismic experiments performed with similar methods in the western part of the East European Craton at the transition to the adjacent Palaeozoic and younger tectonic units (*cf.* Grad *et al.* 2006a). The crustal velocity structure in the middle and lower crust seems to be fairly homogeneous, both vertically and laterally, with few zones of elevated velocity contrast. The situation is different in the upper crust, assumed to occur above the calculated gently inclined seismic velocity discontinuity, descending gradually from a depth of *ca*. 13 km in the south, to *ca*. 23 km in the north of the profile (Fig. 5). The V_p velocity values in the upper crust decrease upwards from *ca*. 6.35 km s^{-1} at its base (Figs 5c and d) to 5.90–5.80 km s^{-1} at the top of the crystalline basement (Figs 5b–d) to 5.40 km s^{-1} in crystalline rocks emerging at the surface. The overlying sedimentary strata are characterised by V_p values of *ca*. 5.15–3.80 km s^{-1} in the Neoproterozoic and Palaeozoic to 2.70–2.30 km s^{-1} in the Mesozoic (Fig. 5b).

Below the discontinuity at 13–23 km the V_p smoothly increases downward, from *ca*. 6.50 to 6.70–6.80 km s^{-1} at the contact with the crustal base (Figs 5c and d), making it difficult to differentiate between the middle and lower crust. The latter difficulty is further aggravated by the fact that no V_p velocity values exceeding 6.90–7.00 km s^{-1} have been recorded even in the lowermost part of the crust, unlike in most other similar profiles shot on the East European Craton (Grad *et al.* 2006a). Similarly, in the horizontal direction there is no clear change in the velocity field (except in the uppermost level—to a depth not exceeding 4 km) when moving laterally from the Precambrian platform into the Neoproterozoic(?) basement of the Variscan/Alpine Fore-Dobrudja Trough and the North Dobrudja Fold-Thrust Belt across the SE extension of the crustal-scale Teisseyre-Tornquist Fault Zone. Thus, on purely seismic grounds it is generally not possible to distinguish these major tectonic units or other types of major structures (fault-bounded blocks or structural complexes), that are known from the surface geological mapping or borehole drilling either in the cratonic or Variscan/Cimmerian crust (Fig. 3). The reason for this lateral velocity homogeneity remains unclear. There is a possibility that the mid-crustal basement rock complexes for both the craton and accreted terranes (of Baltican or peri-Baltican provenance?) may not be different enough compositionally to be distinguishable on a relatively low resolution deep refraction profile.

The most notable peculiarity of the DOBRE-4 profile is that it contains three spectacular successive downward (synformal) bends and upward (antiformal) undulations of the Moho, with their wavelength being of the order of 125–150 km and the amplitude attaining as much as 8–16 km (Figs 5 and 15). In this way, the crustal thickness strongly varies along the profile—from 33–38 km at SP15104 and 15111 to 44–49 km between SP15108 and 15109, and at SP15106. Apart from the Moho undulations, similar wavy aspect, though on a smaller scale, is presented by the seismic velocity model at the upper-crust and upper-mantle levels (Fig. 5).

7.2 Folded Moho

The origin of the semi-periodical undulations of the Moho can hardly be explained by any other mechanism than contractional lithospheric-scale folding (buckling) of the crust and the uppermost mantle. An extensional, rotational faulting hypothesis fails on geometrical reasons due to impossibility to delineate a self-consistent, kinematically linked rotated fault-block system within the overall pattern of seismic V_p velocity field calculated from the DOBRE-4 sounding results (Figs 5 and 15). Similarly, an option of variable crustal thicknesses within particular crustal fault blocks (terranes) of different composition and structure is not supported by a fairly uniform lateral distribution of V_p intervals on the 2-D velocity model section (Fig. 5) and by gradual, wave-shaped changes in the Moho configuration. On the other hand, the results of the

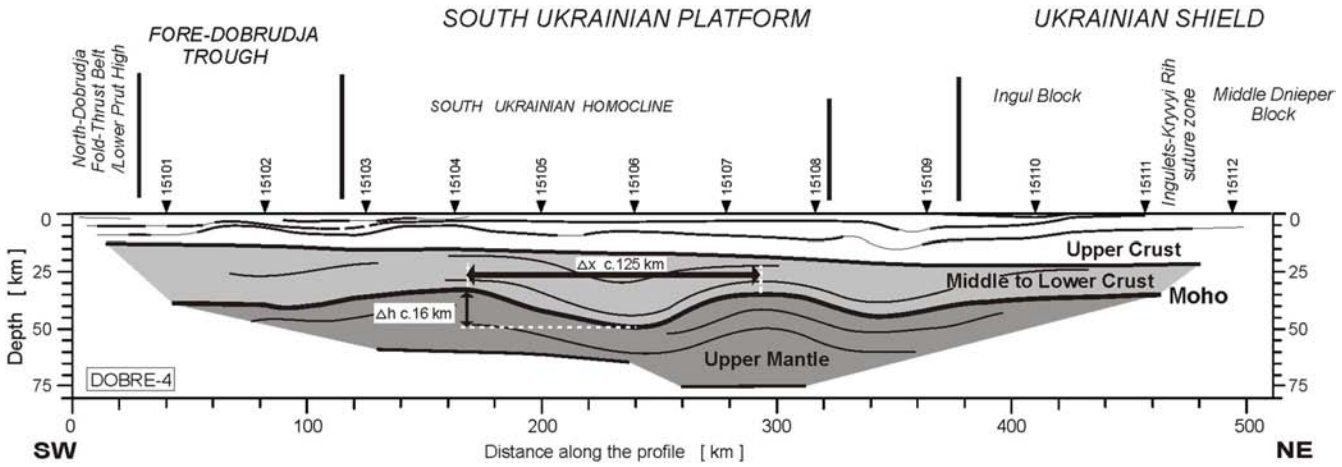

Figure 15. True-shape (not vertically exaggerated) geometry of lithospheric-scale fold structures along the DOBRE-4 profile on schematic section of the upper lithoshere based on *P*-wave velocity seismic model (Fig. 5). Mechanical decoupling along middle/upper crustal detachment (recorded by velocity model) has resulted in different fold wavelengths at lower and upper crustal levels.

nearby, earlier conducted deep reflection seismic study of the Donbas fold belt, named DOBRE (Maystrenko *et al.* 2003), strongly support the buckling hypothesis, in that they have revealed important contractional structures, including a displacement of the Moho by 30–40 km on a large shallow-dipping thrust fault that represents a detachment horizon for a crustal-scale pop-up emergent at the present-day topographic surface.

From the geometrical features of the folded Moho, a bulk tectonic shortening of *ca*. 9.5 per cent due to buckling with respect to its original horizontal length has been estimated, not taking into account the layer-parallel shortening that must have preceded the buckling.

7.3 Lithospheric-scale buckling

The concept of lithospheric-scale compressional folding (buckling) dates back to the 1960s (Biot 1961; Walcott 1970) and since the 1980s it has been more and more seriously considered as a viable, regional-extent mechanism mostly used to explain more or less periodical chains of topographic undulations. The concept has been applied, among others, to the lithosphere of the Indian Ocean (Weissel *et al.* 1980; Gerbault 2000), to the Himalaya and its far-field foreland in Central Asia (e.g. Burov *et al.* 1993; Nikishin *et al.* 1993; Burg & Podladchikov 1999; Caporali 2000; Shin *et al.* 2007), to Australia (Lambeck 1983; Quigley *et al.* 2010) and, in Europe, to the northern foreland of the Alps (Bourgeois *et al.* 2007) and of the Atlas Moutains (the Iberian Peninsula—Cloetingh *et al.* 2002, Muñoz-Martín *et al.* 2010). Comprehensive review papers considering complex thermomechanical aspects of lithosphere-scale folding, its topographic effects and influence on sedimentary basin formation and evolution were published by Cloetingh *et al.* (1999) and by Cloetingh & Burov (2011).

Most of the hitherto published reports of the lithosphere- or crustal-scale folding have been based on interpretation of long-wavelength, periodically alternating topographic elevations and depressions or of fold trains recorded in shallow levels of the crust on geological maps or in reflection seismics. Very few are examples proving the existence of large-scale folds affecting the lower crustal levels, notably the Moho (e.g. Lambeck *et al.* 1988; Goleby *et al.* 1990), using gravimetric measurements. To our knowledge, no such spectacular folds deforming the Moho as those described here, have been yet revealed elsewhere by either deep reflection or refraction seismics.

Based on models of Burov *et al.* (1993), Cloetingh *et al.* (1999) and Cloetingh & Burov (2011) one can describe the Moho folding with a 125–150 km wavelength, accompanied by that of the upper crust with a much shorter wavelength along the DOBRE-4 transect, in terms of 'biharmonic decoupled folding' produced in accordance with the regular, constant wavelength 'linear folding model of Biot (1961)' (Cloetingh *et al.* 1999). Taking, in turn, into account their resemblance to the overall structural patterns produced experimentally by Sokoutis *et al.* (2005), our Moho folds can be explained by 'folding of cold lithosphere with a relatively strong mantle' in the nomenclature of the latter authors.

7.4 Variable scales of fold wavelengths in the crust due to rheological stratification

The DOBRE-4 V_p seismic velocity profile (Fig. 5), apart from the distinct deflections of the Moho, shows numerous, smaller scale velocity field undulations in the upper crust, that can be partly recognized in the configuration of basement-cover boundary and of the sedimentary cover on the near-surface geological cross-section constructed along the DOBRE-4 profile on the basis of borehole data, shallow reflection seismics and surface geological maps (Fig. 3). The gentle undulations in the uppermost crust are restricted to the southern part of the South Ukrainian Homocline, the Fore-Dobrudja Trough and the North Dobrudja Fold-Thrust Belt. They show wavelengths of 8 to 30 km. The shortest-wavelength folds occur in the Palaeozoic through to Late Jurassic sedimentary fill of the Fore-Dobrudja Trough, which itself geometrically is a large-scale syncline, *ca*.120 km wide and more than 3.5 km deep.

The Jurassic accelerated subsidence of the Fore-Dobrudja Trough, that commenced already during Permian–Triassic times (e.g. Gazizova 2009; Ivanova 2011) has been considered as due to either preshortening extension/rifting or compressional (transpression-related?) downfolding (*cf.* Seghedi 2001; Natalin & Şengör 2005).

The specific style and tectonic position of the Fore-Dobrudja Trough, located at the Trans-European suture (Teisseyre-Tornquist Fault Zone) above a depression in Moho topography (Figs 3 and 5), resemble features discovered by Sokoutis *et al.* (2005) in their

analogue models. These models revealed conspicuous single major down-folded and/or down-faulted synclines/pop-downs ('Σ-belts'), overlying Moho synforms, that grew during lithospheric buckling at lithosperic-scale 'suture zones', across which the thickness and rheological properties of the lithosphere changed.

The top of the Precambrian crystalline basement is folded together with the overlying Palaeozoic sequence with wavelengths of 20–30 km; the folds in both sedimentary cover and at top basement are, however, waning to the NE and dying out beyond the SP15105, being replaced by a very gentle homoclinal inclination of the South Ukrainian Homocline and the Ukrainian Shield.

Still in the upper crust, to a depth of *ca*. 10–15 km, fold-like, rather irregular undulations with longer wavelengths (estimated at up to *ca*. 80–120 km) and amplitudes of up to 5 km were calculated in the crystalline basement along the whole length of the DOBRE-4 seismic velocity field profile (Figs 5 and 15). It should be noted, however, that such calculations in rock volumes with slight differences in seismic velocity values, do not necessarily provide unique solutions that precisely portray the real structural geometry of such folds.

7.5 Problem of apparent discordance of folded Moho with the overlying and underlying velocity layers

In the middle and lower crust, below a depth of *ca*. 15 km, subhorizontal attitude of 'velocity layers' with insignificantly different V_p values is envisaged by the calculated seismic model (Fig. 5). Such an attitude of velocity layers does not conform to the geometry of the folded Moho; the layers onlap the Moho in its depressions in a manner similar to that in which sediments are filling a sag basin. Such a flat geometry of velocity layers, instead of one concordant with the undulating Moho, can be explained as due to secondary thermal re-equilibration postdating the crustal folding, which has resulted in restoring the horizontal position of isotherms in compositionally roughly homogeneous lower crust, whereas the Moho deflections have survived thermal re-equilibration, as the Moho represents a distinct compositional boundary. On the other hand, attempts at re-calculation of the seismic velocity model of Fig. 5, in its lower/middle crustal part in such a way that the velocity layering becomes concordant with the shape of the Moho, does not pose particular difficulties, still remaining in agreement with the data acquired in the DOBRE-4 seismic experiment (*cf*. the solution adopted in Fig. 15).

7.6 Deformation partitioning, detachments and possible significance of faulting

The horizontally layered middle/lower crust in the velocity model (Fig. 5) is separated from the overlying undulating upper crust by the already mentioned extremely (unrealistically) extensive, flat-lying discontinuity (detachment horizon), occurring at a depth of *ca*. 13 km in the south, and slowly subsiding to *ca*. 23 km in the north of the profile. The modelled fold chains in the upper crust are dissected as well by a number of subhorizontal, partly folded, seismic velocity discontinuity surfaces.

In one of the velocity models (Fig. 5d) a major south-dipping discontinuity branching off downwards from the Moho, was calculated in the upper mantle. It can indeed represent a large-scale thrust fault that was produced in addition to crustal scale buckle folds to accommodate the overall contractional deformation. It follows from both numerical (e.g. Cloetingh *et al.* 1999; Cloetingh & Burov 2011) and analogue modelling (e.g. Sokoutis *et al.* 2005) that reverse and thrust faults of various dimensions, occurring in the crust and upper mantle, can be involved in and facilitate the process of lithosphere-scale folding. In particular such faults are likely to originate at the inflection points of the growing folds. The activity of major reverse faults during folding often results in formation of pop-up and, especially, conspicuous pop-down structures (Sokoutis *et al.* 2005). Reverse faulting may have played an important role also in the deformation of the crust and mantle investigated by profile DOBRE-4 (*cf*. Fig. 3). However most of such, even major, faults seem to be well beyond the range of resolution of the seismic method applied in our case.

Irrespective of the accuracy of calculations bearing on the precise location and lateral extent of the modelled structures, the presence of several detachment horizons in the folded crust is compatible with the existence of fold systems with various dominant wavelengths at successive crustal levels. Such a situation is considered as typical of lithospheric-scale folding (*cf*. fig. 1 in Cloetingh & Burov 2011) and as reflecting rheological stratification of the lithosphere, where successive competent layers (typically: upper crust, lower crust and upper mantle) suffer significant decrease in strength and increase in ductility towards their basal parts (e.g. Ranalli 1995, 2000). This results in deformation partitioning between particular structural levels, in which competent layers separated by ductile ones are buckled independently, showing wavelengths controlled mostly by their thicknesses (Cloetingh *et al.* 2002; Jarosiński & Dąbrowski 2011; Jarosiński 2012). In our case, as described above, three such mechanically distinct rheological levels can be distinguished, from bottom to top (Fig. 15) corresponding to (1) the uppermost mantle and lower to middle crust (folding the Moho), (2) most of the upper crust, above the 13–23 km detachment and (3) the uppermost crust, above *ca*. 5 km, with the boundary between the two latter layers not clearly recorded in the seismics.

7.7 Dating of the lithospheric buckling

Based on the structural and stratigraphic relationships revealed by the near-surface geological cross-section constructed along the DOBRE-4 profile (Fig. 3), on regional geological situation (Seghedi 2001, 2012; Galetsky 2007; Gazizova 2009) and on results of structural studies carried out in the field (Slyusar' 1984; Hippolyte 2002), it is possible to roughly date the lithosphere-scale folding recorded on the DOBRE-4 profile, assuming the upper crustal folds originated at the same time as those that affected the Moho. The former folds are particularly well developed in the Fore-Dobrudja Trough filled with thick syn-tectonic Triassic-Jurassic deposits. These folds are clearly older than the overlying Oligocene–Neogene strata, defining an unconformable cover along the entire length of the DOBRE-4. Most part of their evolution must have also preceded the deposition of the Cretaceous strata (Fig. 3), the latter presumably being only locally and very slightly affected by folding.

In this way the climax of the folding can be most reliably ascribed to the 'late Cimmerian' transpressional deformation during the end Jurassic to Early Cretaceous (pre-Barremian) that has folded and thrust-faulted the North Dobrudja Fold-Thrust Belt and—to a lesser degree - the Fore-Dobrudja Trough (Slyusar' 1984; Hippolyte 2002; Gazizova 2009). During this deformation the shortening was oriented N–S (Hippolyte 2002) and the Jurassic Callovian (or Oxfordian; Gazizova 2009) rocks became the youngest sediments affected by relatively intense folding.

Following the late Cimmerian compressional event, the area of the Ukrainian Shield and also that of the North Dobrudja Fold-Thrust Belt, remained mostly dry land areas separated by that with marine deposition during Cretaceous times (Galetsky 2007). This may have been due to long-wavelength (*ca*. 500 km) topographic effects of the continuing process of lithosphere-scale buckling, although at a different scale than that responsible for the folds in the Moho, possibly involving the entire thickness of the lithosphere.

During the subsequent deposition of the Upper Cretaceous succession, the Cenomanian through Santonian strata onlapped both the Barremian to Albian cover on the northern rim of the Fore-Dobrudja Trough and the Triassic, Palaeozoic and Precambrian of the northern part of the South Ukrainian Homocline and of the Ukrainian Shield. The Upper Cretaceous sediments in places where they overstep the Fore-Dobrudja Trough and the North Dobrudja Fold-Thrust Belt, are very gently folded (e.g. in the Babadag Basin in Romania; Balintoni *et al.* 2010). This points to the influence the end Cretaceous transregional shortening along the NE–SW direction (as measured in North Dobrudja by Hippolyte 2002) must have had on the tectonic evolution of southern Ukraine. The vigorous end Cretaceous compressional event affected many areas in Europe, leading to widespread inversion and large-scale, mostly open, folding of (Permo-) Mesozoic sedimentary basins (e.g. Mazur *et al.* 2005; Reicherter *et al.* 2008). This tectonic compression of large areal extent has presumably also contributed to the folding of the southern Ukrainian lithosphere. The end-Cretaceous compression, must have uplifted vast areas of southern Ukraine and facilitated the on-going erosion of the Ukrainian Shield. Subsequently, along the entire length of the DOBRE-4 profile moderate subsidence occurred and was accompanied by unconformable deposition of Cenozoic sediments, starting from the Middle Eocene on the South Ukrainian Homocline and the Fore-Dobrudja Trough and from the Oligocene, Miocene or Pliocene on the Ukrainian Shield and the North Dobrudja Fold-Thrust Belt (Galetsky 2007).

A similar, end Cretaceous age was ascribed to the already mentioned mostly brittle, contractional, crustal-scale deformation in the area of Donbas (Donets Basin) by Maystrenko *et al.* (2003), although, a late Cimmerian, Jurassic transpressional event may have also been involved there (*cf.* Saintot *et al.* 2003; Natalin & Şengör 2005). Analogous, Cretaceous, age of lithospheric-scale folding (inferred from large-scale surface folds of wavelengths varying between 50 and 200 km) has been reported from extensive areas of the Arabian Platform (Johnson *vide* Jarosiński & Dąbrowski 2011). The latter folding was associated with a continental collision and involved emplacement of the Oman ophiolite (e.g. Hacker 1994).

It cannot be totally excluded, either, that the intense folding of the Palaeozoic and top Precambrian on the northern limb of the Fore-Dobrudja Trough and the southern part of the South Ukrainian Homocline can be a result of the Variscan compression during the Carboniferous collision with the Moesian Plate across the Dobrudja terranes (*cf.* e.g. Golonka *et al.* 2000; Oczlon *et al.* 2007; Seghedi 2012), with implications concerning the age of the lithospheric folding. It is also true that the folding of the Moho we describe here, being entirely mechanically decoupled from the folds in the upper crust, may have also developed independently and significantly earlier than the latter folds. In this way theoretically considered can also be a hypothetical Precambrian age of the Moho folds, although this would lead to serious difficulties in understanding how they could have survived so long under intense influence of gravity in a viscous medium (*cf.* Cloetingh *et al.* 1999; Cloetingh & Burov 2011; see below).

7.8 Thermomechanical aspects

An estimation of the thermomechanical age (equivalent to 'mechanical mantle thickness' according to Cloetingh *et al.* 1999) of our folded lithosphere has been attempted. Based on our Moho folding wavelength (125–150 km) we arrive at *ca*. 130–200 Ma using the graph of Burov *et al.* (1993; see also fig. 1 in Cloetingh *et al.* 1999, and fig. 3 in Cloetingh & Burov 2011). If then, using this result, we arbitrarily assume that last thermal re-equilibration of the local lithosphere occurred during Late Carboniferous–Early Permian (300–280 Ma), following the Gondwana–Laurussia collision across the Teisseyre–Tornquist suture, our lithosphere buckling can be expected to have occurred within a time span of *ca*. 170 to 80 Ma. This contains end Jurassic-earliest Cretaceous time interval (*ca*. 155–130 Ma), which we consider here as the most probable timing for the buckling. The assumed hypothetical Variscan heating following the Pangaea assembly must have been areally extensive, to be able to affect laterally the Precambrian lithosphere of the East European Craton to a distance of at least 500 km. A further speculation is that this heating must have been as intense as to promote lateral gravitational spreading and thinning of the thick Precambrian crust, in particular of its lower part (*cf.* Rey *et al.* 2001), and have thus lead to the current uniform subhorizontal seismic layering and lateral homogeneity of the lower and middle crust observed across the Precambrian and Palaeozoic/Mesozoic crustal units (Fig. 5).

One can also try to estimate the thickness of a competent layer in the upper mantle/lower crust, the folding of which would produce folds with a given constant wavelength. Assuming the typical value of $\lambda/h = 4$–6, where λ is the dominant wavelength and h is the thickness of the competent layer under influence of gravity, and the typical viscosity ratio $\mu_c/\mu_e = 100$, where indices c and e stand for the competent layer and its embedding material, respectively (Cloetingh *et al.* 1999), the thickness of the folded uppermost mantle competent layer is estimated at 20–37 km, using the graph of Cloetingh *et al.* (1999, their fig. 3A). This is in agreement with one of lithospheric effective elastic thickness, T_e, determinations for the Scythian Platform and the directly adjacent margin of the East European Craton made by Pérez-Gussinyé & Watts (2005). Using the Bouguer coherence method for entire Europe, they arrived at an anomalously thin T_e of 20–40 km in the area in question. This value is similar to that of the Variscan and northern Alpine Europe and in strong contrast with $T_e > 70$ km for most of the East European Platform north of the Dnieper-Donets Basin.

In this way, the estimated thermomechanical age of our folded lithospheric competent layer would be relatively young and its thickness small. At the same time, however, predictions concerning a possible preservation of lithosphere-scale folding effects over 'large time spans', that is, exceeding 20 Myr require 'strong rheology lithosphere', equivalent to that obtained for a thermal age in excess of 700–1000 Ma (Cloetingh *et al.* 1999), which is at odds with our estimations of a young thermomechanical age and small thickness of the competent part of our folded lithosphere on the basis of the Moho folds wavelength. The latter two features seem to contradict, as well, the model of folding of a cold lithosphere with a relatively strong mantle, which we inferred from the modelling results of Sokoutis *et al.* (2005). Therefore, a possibility should be considered that the Moho folds recorded by the DOBRE-4 profile did not behave during deformation according to the regular, linear (Biot's 1961) model, with the implication that the resultant fold wavelength may not be directly dependent on the thermomechanical lithospheric age/competent layer thickness.

On the other hand, the distinct Cenozoic and Cretaceous thickness changes, together with the top-Precambrian topography considered on the scale of the entire DOBRE-4 profile (Fig. 3) can be alternatively interpreted in terms of a prolonged compression, acting roughly continuously since Triassic(?)–Jurassic times until recently. Indeed, sparse data concerning North Dobrudja and the NW Black Sea included in the World Stress Map (Heidbach *et al.* 2008) seem to point to a maximum horizontal compressive stress still acting in the uppermost crust in the direction of NE–SW to E–W, that is in the direction presumably favourable for supporting our folds in the Moho. Such a long-term compression may have prevented the Moho folds relaxation, even if they occurred in a thermomechanically young lithosphere.

We admit the above problems deserve further attention and study, including modelling the rheology and structure of the litosphere up to its very base and interpreting other types of geophysical data.

7.9 Geodynamic scenario

The geodynamic scenario for the large-scale folding recorded in profile DOBRE-4 must have been related to the tectonic plate kinematics in this part of Europe during Triassic through beginning Tertiary times. The present-day knowledge, however, on the complex details of changing plate configurations during closing of the Neotethys and of the local oceans of Meliata, Maliac, Pindos and Vardar, as well as during the opening of the Black Sea and the concomitant collisions of the continental masses and slivers, all occurring in close vicinity of the studied area, remains fairly obscure and controversial (e.g. Stampfli & Borel 2002; Golonka 2004; Schmid *et al.* 2008; Kalvoda & Bábek 2010). The continental sliver of the North Dobrudja Fold-Thrust Belt, with original Variscan orogenic structure, became involved in early Alpine (Cimmerian) events and experienced extension during Late Permian–Middle Triassic times, and, subsequently, compression (transpression) in the Late Triassic–Middle Jurassic (Seghedi 2001, 2012). In the Late Jurassic-beginning Cretaceous (Slyusar' 1984; Hippolyte 2002) it was pushed from the south by its rigid neighbour—the Moesian platform in a context of subduction-related closing of the nearby local oceanic basins (Stampfli & Borel 2002; Golonka 2004). It must then have exerted compression on the adjacent Fore-Dobrudja Trough with its crystalline basement, representing the marginal part of the East European Craton affected by the Variscan and Cimmerian tectonism (the Scythian Platform). The compression was associated with strike-slip displacements on the crustal-scale NW–SE trending faults cutting across the North Dobrudja Fold-Thrust Belt and separating it from the Scythian Platform (Hippolyte 2002; Kalvoda & Bábek 2010; Seghedi 2012). In Early Cretaceous times, some 200 km SE of the DOBRE-4 profile the western Black Sea began to open (Munteanu *et al.* 2011) and a major splinter of Variscan continental crust, originally located adjacent to the present-day Odessa Shelf, became separated from the Moesian Platform, North Dobrudja and Fore-Dobrudja Trough areas (Okay *et al.* 1994; Kalvoda & Bábek 2010). This was due to northward subduction of the local Intra-Pontide oceanic lithosphere below it and the resultant backarc spreading at the edge of the Odessa Shelf. The splinter migrated as far as 300 km to the SSW until Eocene times, leaving behind the newly opened oceanic tract of the Western Black Sea basin and, eventually, docked to the Anatolian collage as the Istanbul–Zonguldak terrane (Okay *et al.* 1994).

These significant tectonic events must have had a direct influence on the neighbouring part of the East European Craton and the adjacent tectonic units, leading to the end Jurassic-Early Cretaceous crustal folding and concomitant uplift of the Ukrainian Shield and of the Dobrudja Fold-Thrust Belt together with the Fore-Dobrudja Trough. This was followed by mid- to Late Cretaceous subsidence of the areas along the central part of the DOBRE-4 profile and intense erosion of the uplifted shield, preceding a strong end-Cretaceous compressional paroxysm along the NE–SW axis, which may have also contributed to the crustal-scale buckling in the region. Subsequently, during Palaeogene times, the uplifted areas became mostly levelled, subsided and buried by extensive, though not thick, Oligocene–Miocene to Quaternary sedimentary cover.

ACKNOWLEDGEMENTS

Fieldwork and data acquisition in the DOBRE-4 profile were carried out in an international multilateral collaboration. We offer our sincere thanks to the many people and organisations from Denmark, Finland, Poland and Ukraine who have contributed to DOBRE-4, especially technical experts who participated in the fieldwork. We greatly appreciate the constructive and helpful review by Sierd Cloetingh as well as fruitful discussions on lithospheric folding with Marcin Dąbrowski and Marek Jarosiński. Tesseral Technologies Inc. developed the software for full wave modelling. We express our gratitude to their staff for technical support. The public domain GMT package (Wessel & Smith 1995) was used to produce some of the maps.

REFERENCES

Balintoni, I., Balica, C., Seghedi, A. & Ducea, M.N., 2010. Avalonian and Cadomian terranes in North Dobrogea, Romania, *Precambrian Res.*, **182,** 217–229.

Biot, M.A., 1961. Theory of folding of stratified viscoelastic media and its implications in tectonics and orogenesis, *Geol. Soc. Am. Bull.*, **72,** 1595–1620.

Bogdanov, A.A., Muratov, M.V. & Schatsky, N.S. (Eds), 1964. *The Tectonics of Europe. Explanatory Note to International Geological Map 1 : 2 500 000 and Explanatory Note*. Int. Geol. Congress, Comission on the Geological Map of the World, Nauka, 364 p. (in Russian).

Bogdanova, S.V., 2005. The East European Craton: some aspects of the Proterozoic evolution in its south-west, *Mineral. Soc. Poland–Spec. Papers*, **26,** 18–24.

Bogdanova, S.V., Pashkevich, I.K., Gorbatschev, R. & Orlyuk, M.I., 1996. Riphean rifting and major Palaeoproterozoic crustal boundaries in the basement of the East European Craton: geology and geophysics, *Tectonophysics*, **268,** 1–21.

Borodulin, M.A. & Baysarovich, M.N., 1992. The model of the lithosphere of the Ukrainian shield based on CDP data, *Geophys. J. (Kiev)*, **14**(4), 56–66 (in Russian).

Bourgeois, O., Ford, M., Diraison, M., Le Carlier de Veslud, C., Gerbault, M., Pik, R., Rub, N. & Bonnet, S., 2007. Separation of rifting and lithospheric folding signatures in the NW-Alpine foreland, *Int. J. Earth Sci.*, **96**(6), 1003–1031.

Burg, J.-P. & Podladchikov, Yu., 1999. Lithospheric scale folding: numerical modelling and application to the Himalayan syntaxes, *Int. J. Earth Sci.*, **88,** 190–200.

Burov, E.B., Lobkovsky, L.I., Cloetingh, S. & Nikishin, A.M., 1993. Continental lithosphere folding in central Asia, part II: constraints from gravity and topography, *Tectonophysics*, **226,** 73–87.

Caporali, A., 2000. Buckling of the lithosphere in western Himalaya: constraints from gravity and topography data, *J. geophys. Res.*, **105,** 3103–3113.

Červený, V. & Pšenčík, I., 1984. SEIS83—numerical modelling of seismic wave fields in 2-D laterally varying layered structures by the ray method,

in *Documentation of Earthquake Algorithms*, Rep. SE-35, pp. 36–40, ed. Engdal, World Data Center (A) for Solid Earth Geophysics.

Chekunov, A.V., 1988. *Lithosphere of Central and Eastern Europe. Geotraverse IV, VI, VIII*, Naukova Dumka, 170 pp. (in Russian).

Chekunov, A.V., Sollogub, V.B., Galetsky, L.S. & Kurlov, N.S., 1989. Geodynamic model of the central part of the Ukrainian Shield and Kryvyi Rig ultradeep borehole, *Geophys. J. (Kiev)*, **11**(4), 3–13 (in Russian).

Chekunov, A.V., Kivshik, N.K., Omelchenko, V.D. & Tolkunov, A.P., 1992. Putivl-Krivoy Rog DSS profile across ultra-deep wells in Ukraine, *Geophys. J. (Kiev)*, **14**(1), 3–10 (in Russian).

Cloetingh, S. & Burov, E., 2011. Lithospheric folding and sedimentary basin evolution: a review and analysis of formation mechanisms, *Basin Res.*, **23,** 257–290.

Cloetingh, S., Burov, E. & Poliakov, A., 1999. Lithosphere folding: primary response to compression? (from Central Asia to Paris Basin), *Tectonics*, **18,** 1064–1083.

Cloetingh, S., Burov, E., Beekman, F., Andeweg, B., Andriessen, P.A.M., Garcia-Castellanos, D., Vicente, G. & Vegas, R., 2002. Lithospheric folding in Iberia, *Tectonics*, **21**(5), 1041, doi:10.1029/2001TC901031.

DOBREfraction'99 Working Group, Grad, M. *et al.*, 2003. "DOBREfraction'99"—velocity model of the crust and upper mantle beneth the Donbas Foldbelt (East Ukraine), *Tectonophysics*, **371,** 81–110.

Egorkin, A.V., 1966. Analysis of the accuracy determination of velocity cross-section in the Earth's crust from travel time of reflected waves. Izv. Akad. Nauk SSSR, *Fizika Zemli*, **9,** 72–81 (in Russian).

Galetsky, L.S. (Ed.), 2007. *An Atlas of the Geology and Mineral Deposits of Ukraine*, University of Toronto Press, 168 pp.

Gazizova, S.A., 2009. Towards a comparative analysis of basins surrounding the East-European Platform. The Dobrudja Foredeep Basin, *Geologicheskiy sbornik Instituta Geologii Ufimskogo Nauchnogo Centra Rossiyskoy Akademii Nauk* No. 8, 88–93, Ufa (in Russian).

Gerbault, M., 2000. At what stress level is the central Indian Ocean lithosphere buckling? *Earth planet. Sci. Lett.*, **178**(1/2), 165–181.

Gintov, O.B., 2005. *Field Tectonophysics and its Application in the Studies of Deformations of the Earth's Crust in Ukraine*, Feniks, 572 pp. (in Russian).

Gintov, O.B. & Mychak, S.V., 2011a. Geodynamic development of the Ingul megablock of the Ukrainian Shield according to geological-geophysical and tectonophysical data. Part 1, *Geophys. J. (Kiev)*, **33**(3), 102–118 (in Russian).

Gintov, O.B. & Mychak, S.V., 2011b. Geodynamic development of the Ingul megablock of the Ukrainian Shield according to geological-geophysical and tectonophysical data. Part 2, *Geophys. J. (Kiev)*, **33**(4), 41–58 (in Russian).

Goleby, B.R., Kennett, B.L.N., Wright, C., Shaw, R.D. & Lambeck, K., 1990. Seismic reflection profiling in the Proterozoic Arunta Block, central Australia: processing for testing models of tectonic evolution, *Tectonophysics*, **173,** 257–268.

Golonka, J., 2004. Plate tectonic evolution of the southern margin of Eurasia in the Mesozoic and Cenozoic, *Tectonophysics*, **381,** 235–273.

Golonka, J., Oszczypko, N. & Ślączka, A., 2000. Late Carboniferous-Neogene geodynamic evolution and paleogeography of the circum-Carpathian region and adjacent areas, *Ann. Soc. Geol. Pol.*, **70,** 107–136.

Gorbatchev, R. & Bogdanova, S., 1993. Frontiers in the Baltic Shield, *Precambrian Res.*, **64,** 3–22.

Grad, M., 1983. Determination of mean velocities and depths of boundaries in the Earth's crust from reflected waves, *Acta geophys. Pol.*, **31,** 231–241.

Grad, M. & Tripolsky, A.A., 1995. Crustal structure from P and S seismic waves and petrological models of the Ukrainian shield, *Tectonophysics*, **250,** 89–112.

Grad, M. *et al.*, 2003a. Crustal structure of the Trans-European suture zone region along POLONAISE'97 seismic profile P4, *J. geophys. Res.*, **108**(B11), 2541, doi:10.1029/2003JB002426.

Grad, M. *et al.*, 2003b. DOBRE-99: the crust structure of the Donets Basin along the Mariupol-Belovodsk profile, *Izvestiya, Phys. Solid Earth*, **39,** 464–473.

Grad, M. *et al.*, 2006a. Lithospheric structure beneath trans-Carpathian transect from Precambrian platform to Pannonian basin: CELEBRATION 2000 seismic profile CEL05, *J. geophys. Res.*, **111,** B03301, doi:10.1029/2005JB003647.

Grad, M., Janik, T., Guterch, A., Środa, P., Czuba, W. & EUROBRIDGE'94–97, POLONAISE'97 & CELEBRATION 2000 Seismic Working Groups, 2006b. Lithospheric structure of the western part of the East European Craton investigated by deep seismic profiles, *Geol. Quart.*, **50**(1), 9–22.

Grad, M., Guterch, A., Mazur, Z., Keller, G.R., Špičák, A., Hrubcová, P. & Geissler, W.H., 2008. Lithospheric structure of the Bohemian Massif and adjacent Variscan belt in central Europe based on profile S01 from the SUDETES 2003 experiment, *J. geophys. Res.*, **113,** B10304, doi:10.1029/2007JB005497.

Guterch, A., Grad, M., Materzok, R. & Perchuć, E., 1986. Deep structure of the earth's crust in the contact zone of the palaeozoic and precambrian platforms in Poland (Tornquist-Teisseyre zone), *Tectonophysics*, **128,** 251–279.

Guterch, A., Grad, M. & Keller, G.R., 2007. Crust and lithospheric structure—long range controlled source seismic experiments in Europe, in *Treatise on Geophysics*, Vol. 1, pp. 533–558, eds Schubert, G., Romanowicz, B. & Dziewonski, A., Elsevier.

Hacker, B.R., 1994. Rapid emplacement of young oceanic lithosphere: argo geochronology of the Oman Ophiolite, *Science*, **265,** 1563–1565.

Hansen, T.M. & Jacobsen, B.H., 2002. Efficient finite difference waveform modeling of selected phases using a moving zone, *Comput. Geosci.*, **28**(7), 819–826.

Hauser, F., Raileanu, V., Fielitz, W., Dinu, C., Landes, M., Bala, A. & Prodehl, C., 2007. Seismic crustal structure between the Transylvanian Basin and the Black Sea, Romania, *Tectonophysics*, **430,** 1–25.

Heidbach, O., Tingay, M., Barth, A., Reinecker, J., Kurfeß, D. & Müller, B., 2008. The World Stress Map database release 2008; doi:10.1594/GFZ.WSM.Rel.2008. Available at: http://dc-app3-14.gfz-potsdam.de/ (last accessed 22 August 2013).

Hippolyte, J.-C., 2002. Geodynamics of Dobrogea (Romania): new constraints on the evolution of the Tornquist-Teisseyre Line, the Black Sea and the Carpathians, *Tectonophysics*, **357,** 33–53.

Ivanova, A.V., 2011. Catagenesis of Phanerozoic rocks of the area between the Dnieper and Prut as a result of pecularities of its geological evolution, *Dopovidy Nacionalnoy Akademii Nauk Ukrainy*, **2011**(1), 91–97 (in Russian).

Janik, T., Yliniemi, J., Grad, M., Thybo, H., Tiira, T. & POLONAISE P2 Working Group, 2002. Crustal structure across the TESZ along POLONAISE'97 seismic profile P2 in NW Poland, *Tectonophysics*, **360,** 129–152.

Janik, T., Grad, M., Guterch, A. & CELEBRATION 2000 Working Group, 2009. Seismic structure of the lithosphere between the East European Craton and the Carpathians from the net of CELEBRATION 2000 profiles in SE Poland, *Geol. Quart.*, **53**(1), 141–158.

Jarosiński, M., 2012. Compressive deformations and stress propagation in intracontinental lithosphere: finite element modeling along the Dinarides-East European Craton profile, *Tectonophysics*, **526–529,** 24–41.

Jarosiński, M. & Dąbrowski, M., 2011. Final report on research project no N N307 116235: Topographic effects and folding mechanisms of rheologically delaminated lithosphere: modeling with finite element method (unpublished material; in Polish), Archives of Polish Geological Institute, Warszawa, 139 pp.

Kalvoda, J. & Bábek, O., 2010. The margins of Laurussia in central and southeast Europe and southwest Asia, *Gondwana Res.*, **17,** 526–545.

Khain, V.E., 1977. *Regional Geotectonics. Europe Outside the Alps and Western Asia*, Nedra, 359 pp. (in Russian).

Khomenko, V.I., 1987. *Deep Structure of the South-Western Edge of the East-European Platform*, Naukova Dumka, 140 pp. (in Russian).

Kolomiyets, A.V. & Kharchenko, A.V., 2008. Tuning parallel computations for low-bandwidth network, *Comput. Math.*, **1,** 63–69 (in Russian).

Komminaho, K., 1998. Software Manual for Programs MODEL and XRAYS: A Graphical interface for SEIS83 Program Package, University of Oulu, Dep. of Geophys., Rep. 20, 31 pp.

Kostyukevich, A.S., Starostenko, V.I. & Stephenson, R.A., 2000. The full-wave images of the models of the deep lithosphere structures constructed according to DSS and CDP data interpretation, *Geophys. J. (Kiev)*, **22**(4), 96–98.

Kruglov, S.S., 2001. *The Problems of Tectonics and Paleogeodynamics of Western Ukraine* (A critical survey of new publications), Interdepartmental Tectonic Committee of Ukraine, 83 pp.

Kruglov, S.S. & Tsypko, A.K., 1988. *Tectonics of Ukraine*, Nedra, 254 pp. (in Russian).

Kruglov, S.S. & Gursky, D.S., 2004. Tectonic Map of the Ukraine. M 1:1000000. Edition of State Geol. Survey., Kiev, pp. 3–21 (in Russian).

Kruglov, S.S. & Gursky, D.S., 2007. Tectonic Map of the Ukraine. M 1:1000000, Explanatory note, P.1, Ministry of Environmental Protection, State Geol. Survey, Ukr. DGRI, 96 pp. (in Russian).

Lambeck, K., 1983. The role of compressive forces in intracratonic basin formation and mid-plate orogenies, *Geophys. Res. Lett.*, **10**(9), 845–848.

Lambeck, K., Burgess, G. & Shaw, R.D., 1988. Teleseismic travel-time anomalies and deep crustal structure in central Australia, *Geophys. J. R. astr. Soc.*, **94,** 105–124.

Maystrenko, Yu., Stovba, S. & Stephenson, R., 2003. Crustal-scale pop-up structure in cratonic lithosphere: DOBRE seismic reflection study of the Donbas fold belt, Ukraine, *Geology*, **31,** 733–736.

Mazur, S., Scheck-Wenderoth, M. & Krzywiec, P., 2005. Different modes of the Late Cretaceous–Early Tertiary inversion in the North German and Polish basins, *Int. J. Earth Sci.*, **94,** 782–798.

Milanovsky, E.E., 1996. *Geology of Russia and Adjacent Areas (Northern Eurasia)*, Moscow University Press, 448 pp. (in Russian).

Mizerski, W. & Stupka, O., 2005. Western and southern extent of the East European Craton, *Przegląd Geologiczny*, **53**(11), 1030–1039 (in Polish).

Muñoz-Martín, A., De Vicente, G., Fernández-Lozano, J., Cloetingh, S., Willingshofer, E., Sokoutis, D. & Beekman, F., 2010. Spectral analysis of the gravity and elevation along the western Africa–Eurasia plate tectonic limit: Continental versus oceanic lithospheric folding signals, *Tectonophysics*, **495**(3–4), 298–314.

Munteanu, I., Matenco, L., Dinu, C. & Cloetingh, S., 2011. Kinematics of back-arc inversion of the Western Black Sea Basin, *Tectonics*, **30,** TC5004, doi:10.1029/2011TC002865.

Natalin, B.A. & Şengör, A.M.C., 2005. Late Palaeozoic to Triassic evolution of the Turan and cythian platforms: The pre-history of the Palaeo-Tethyan closure, *Tectonophysics*, **404,** 175– 202.

Nikishin, A.M., Cloetingh, S., Lobkovsky, L. & Burov, E.B., 1993. Continental lithosphere folding in central Asia, part I, Constraints from geological observations, *Tectonophysics*, **226,** 59–72.

Nikishin, A.M. *et al.*, 1996. Late Precambrian to Triassic history of the East European Craton: dynamics of sedimentary basin evolution, *Tectonophysics*, **268,** 23–63.

Nikishin, A.M. *et al.*, 2001. Mesozoic and Cenozoic evolution of the Scythian Platform-Black Sea-Caucasus domain, in *Peri-Tethys Memoir 6. PeriTethyan Rift /Wrench Basins and Passive Margins*, Vol. 186, pp. 295–346, eds Ziegler, P.A., Cavazza, W., Robertson, A.H.F. & Crasquin-Solau, S., Mémoires du Musée National d'Histoire Naturelle.

Oczlon, M.S., Seghedi, A. & Carrigan, C.W., 2007. Avalonian and Baltican terranes in the Moesian Platform (southern Europe, Romania and Bulgaria) in the context of Caledonian terranes along the Southwestern margin of the East European craton, in *The Birth of the Rheic Ocean: From Avalonian-Cadomian Active Margin to the Allengian-Variscan Collision*, Vol. 423, pp. 375–400, eds Linnemann, U., Nance, R.D., Kraft, P. & Zulauf, G., Geological Society of America, Special Paper.

Okay, A.I., Şengör, A.M.C. & Görür, N., 1994. Kinematic history of the opening of the Black Sea and its effect on the surrounding regions, *Geology*, **22,** 267–270.

Pérez-Gussinyé, M. & Watts, A.B., 2005. The long-term strength of Europe and its implications for plate-forming processes, *Nature*, **436,** 381–384.

Pharaoh, T.C., 1999. Palaeozoic Terranes and their lithospheric boundaries within the Trans-European Suture Zone, TESZ, a review, *Tectonophysics*, **314,** 17–41.

Quigley, M.C., Clark, D. & Sandiford, M., 2010. Tectonic geomorphology of Australia, *Geol. Soc., Lond., Spec. Publ.*, **346,** 243–265.

Ranalli, G., 1995. *Rheology of the Earth*, 2nd edn, Chapman and Hall, 413 pp.

Ranalli, G., 2000. Rheology of the crust and its role in tectonic reactivation, *J. Geodyn.*, **30,** 3–15.

Reicherter, K. *et al.*, 2008. Alpine tectonics north of the Alps, in *The Geology of Central Europe. Volume 2: Mesozoic and Cenozoic*, pp. 1233–1285, ed. McCann, T., Geological Society.

Rey, P., Vanderhaeghe, O. & Teyssier, C., 2001. Gravitational collapse of the continental crust: definition, regimes and modes, *Tectonophysics*, **342,** 435– 449.

Saintot, A., Stephenson, R., Stovba, S. & Maystrenko, Y., 2003. Structures associated with inversion of the Donbas Foldbelt (Ukraine and Russia), *Tectonophysics*, **373,** 181–207.

Saintot, A., Stephenson, R.A., Stovba, S., Brunet, M.-F., Yegorova, T. & Starostenko, V., 2006. The evolution of the southern margin of Eastern Europe (Eastern European and Scythian platforms) from the latest Precambrian-Early Palaeozoic to the Early Cretaceous, in *European Lithosphere Dynamics*, Vol. 32, pp. 481–505, eds Gee, D.G. & Stephenson, R.A., Geological Society, Memoirs.

Schatsky, N.S., Stillle, H., Bogdanov, A.A. & Blundell, F. (Eds), 1962. *The Tectonics of Europe. International Geological Map 1 : 2 500 000*. Int. Geol. Congress, Comission on the Geological Map of the World. Academy of Sciences of U.S.S.R. (in Russian).

Scherbak, N.P., 2005. *Early Precambrian of the Ukrainian Shield*, Archaean. Naukova Dumka, 244 pp. (in Russian).

Scherbak, N.P., 2008. *Early Precambrian of the Ukrainian Shield*, Proterozoic. Naukova Dumka, 240 pp. (in Russian).

Schmid, S., Bernoulli, D., Fügenschuh, B., Matenco, L., Schefer, S., Schuster, R., Tischler, M. & Ustaszewski, K., 2008. The Alpine-Carpathian-Dinaridic orogenic system: correlation and evolution of tectonic units, *Swiss J. Geosci.*, **101,** 139–183.

Seghedi, A., 2001. The North Dobrogea orogenic belt (Romania): a review, in *Peri-Tethys Memoir 6: PeriTethyan Rift /Wrench Basins and Passive Margins*, Vol. 186, pp. 237–257, eds Ziegler, P.A., Cavazza, W., Robertson, A.F.H. & Crasquin-Soleau, S., Memoires du Museum national d'Histoire naturelle.

Seghedi, A., 2012. Palaeozoic formations from Dobrogea and Pre-Dobrogea—an overview, *Turkish J. Earth Sci.*, **21,** 669–721.

Seghedi, A., Berza, T., Iancu, V., Mărunţiu, M. & Oaie, G., 2005. Neoproterozoic terranes in the Moesian basement and in the Alpine Danubian nappes of the South Carpathians, *Geol. Belg.*, **8,** 4–19.

Sharov, N.V., 2004. *Deep Structure and Seismicity of the Karelian Region and its Surroundings*, Karelian Research Center, 353 pp. (in Russian).

Shin, Y.H., Xu, H., Braitenberg, C., Fang, J. & Wang, Y., 2007. Moho undulations beneath Tibet from GRACE-integrated gravity data, *Geophys. J. Int.*, **170,** 971–985.

Slyusar', B.S., 1984. Structures of the horizontal compression in the northern Fore-Dobrudja, *Geotektonika*, **4,** 90–105 (in Russian).

Sokoutis, D., Burg, J.-P., Bonini, M., Corti, G. & Cloetingh, S., 2005. Lithospheric-scale structures from the perspective of analogue continental collision, *Tectonophysics*, **406,** 1–15

Sollogub, V.B., 1982. Earth's crust of the Ukraine, *Geophys. J.*, **4**(4), 3–25.

Sollogub, V.B., 1986. *Lithosphere of the Ukraine*, Naukova Dumka, 184 pp. (in Russian).

Sollogub, V.B., Chekunov, A.V. & Kaluznaya, L.T., 1988. Lithosphere structure along the geotraverse II, in *Lithosphere of Central and East Europe. Geotraverse I, II, V*, pp. 63, Naukova Dumka (in Russian).

Środa, P. *et al.*, 2006. Crustal structure of the Western Carpathians from CELEBRATION 2000 profiles CEL01 and CEL04: seismic models and geological implication, *Geophys. J. Int.*, **167,** 737–760.

Stampfli, G.L. & Borel, G.D., 2002. A plate tectonic model for the Palaozoic and Mesozoic constrained by dynamic plate boundaries and restored synthetic oceanic isochrons, *Earth planet. Sci. Lett.*, **196,** 17–33.

Starostenko, V. *et al.*, 2013. Seismic velocity model of the crust and upper mantle along profile PANCAKE across the Carpathians between

the Pannonian Basin and the East European Craton, *Tectonophysics*, doi:10.1016/j.tecto.2013.07.008.

Starostenko, V.I., Kazanskiy, V.I., Drogitskaya, G.M., Makivchuk, O.F., Popov, N.I., Tarasov, N.N., Tripolskiy, A.A. & Sharov, N.V., 2007. Relationship of surficial structures of the Kirovograd ore area (the Ukrainian Shield) with local heterogeneities of the crust and the relief of Moho discontinuity, *Geophys. J. (Kiev)*, **29,** 1 (in Russian).

Walcott, R.I., 1970. Flexural rigidity, thickness, and viscosity of the lithosphere, *J. geophys. Res.*, **75,** 3941–3954.

Weissel, J.K., Anderson, R.N. & Geller, C., 1980. Deformation of the Indo-Australian plate, *Nature*, **287,** 284–291.

Wessel, P. & Smith, W.H.F., 1995. New version of the Generic Mapping Tools released, *EOS, Trans. Am. geophys. Un.*, **76,** 329.

Zelt, C.A., 1994. *Software Package ZPLOT,* Bullard Laboratories, University of Cambridge.